Pool boiling on vertical and horizontal heated plates with a dielectric fluid: Influence of vertical canal width

Antonio Della Volpe, Nicolas Baudin, Stéphane Roux, Robert Yu, Jean-Michel Fiard, Jérôme Bellettre

Pool boiling on vertical and horizontal heated plates with a dielectric fluid: influence of vertical canal width

Antonio della Volpe[1,2], Nicolas Baudin[1], Stéphane Roux[1], Robert Yu[2], Jean-Michel Fiard[2], Jérôme Bellettre[1]

1 - LTEN UMR 6607 CNRS, Nantes Université, Rue Christian Pauc, Nantes, 44300, France

2 - RENAULT GROUP, 1 Avenue du Golf, Guyancourt, 78280, France

Corresponding author: Nicolas Baudin

Mail: nicolas.baudin@univ-nantes.fr Tel: +33240683131

Other authors mail : antonio.della-volpe@univ-nantes.fr, nicolas.baudin@univ-nantes.fr, stephane.roux@univ-nantes.fr, robert.yu@renault.com, jean-michel.fiard@renault.com, jerome.bellettre@univ-nantes.fr

Keywords

Pool boiling, confinement, two-phase heat exchange, critical heat flux

Abstract

A closed system testbench has been developed to study pool boiling with a dielectric fluid at atmospheric pressure. The experimental setup consists in immerged horizontal and vertical adjacent heated plates, representing the corner of a parallelepipedal heating element. Both plates are 64x40mm². The plates can be heated separately or simultaneously, with surface heat flux ranging from 0 to 20 W/cm^2. Additionally, the canal width in front of the vertical heated plate is varied from 0.5 to 15 mm to study the influence of confinement. The opposite wall of the canal is made of transparent glass to allow optical visualization of the boiling on the vertical plate. A condenser at the top of the system controls the fluid subcooling. The wall temperatures are measured in steady-state regime in the middle of the plates, heat transfer coefficients are also determined. This configuration leads to complex flows, from natural convection to film boiling, including nucleate boiling. For low heat flux, smaller vertical canal widths enhance natural convection mixed with phase change phenomena: this conveys significantly higher heat transfer coefficients than in the vertical free configuration case. At higher heat flux, confinement does not enhance heat exchange on the vertical plate. When the vertical plate is confined, bubble coalescence and critical heat flux occur for lower heat flux compared to the free configuration. Visual observations on boiling regimes on the vertical

plate are given depending on confinement. Finally, simultaneous heating of both plates is compared to isolated plate heating: boiling on the vertical plate improves heat exchange on the horizontal one, whereas boiling on the horizontal plate has no effect on the vertical one.

Nomenclature

Variable	Physical quantity	Unit (SI)
C_p	Heat capacity	J/(K.kg)
CHF	Critical heat flux	W/m²
d_{tr}	Transition distance (microscale to macroscale)	m
e	Confinement, canal width	m
g	Gravitational acceleration	m/s²
H	Height of heated plate	m
h	Heat transfer coefficient	W/(K.m²)
L	Width of heated plate	m
L_{cap}	Capillary length	m
P	Pressure	Pa
q''	Surface heat flux	W/m²
Ra	Rayleigh number	-
R_{th}	Thermal resistance	K/W
S	Surface of heated plate	m²
T	Temperature	K
TCONB	Thermocouple of boiling (incipience)	-
$u()$	Uncertainty of variable	-
Z	Surface rugosity	µm

Subscripts	Physical quantity	Unit (SI)
∞	Far from the plate	-
cond	Condenser	-
elec	Electrical (power input)	-
f	Fluid	-
H	Horizontal plate	-
h	Heater	-
l	Liquid state	-
NB	Nucleate boiling	-
NC	Natural convection	-
ONB	Onset of boiling	-
sub	Subcooling	-
sat	Saturation state	-
V	Vertical plate	-
v	Vapor state	-

Greek letters	Physical quantity	Unit (SI)
α	Thermal diffusivity	m^2/s
β	Thermal expansion coefficient	K^{-1}
Δh_{lv}	Liquid-vapor latent heat	J/kg
ΔT	Temperature difference	K
λ	Thermal conductivity	W/(m.K)
μ	Dynamic viscosity	Pa.s
ρ	Mass density	kg/m^3
σ	Surface tension	J/m^2
θ	Contact angle	°

Introduction

Pool boiling is one of the most effective means to exchange heat from a solid surface to a fluid without providing external work. This is possible thanks to the phase change phenomenon absorbing the heat, plus the convection flows which have amplified heat transfer coefficients in bubbly flows [1]. The advantages of pool boiling are the cooling system simplicity of design, which consists in an evaporator (the object we want to extract heat from), the fluid and a condenser (which removes the heat from the system). On the other hand, it is important to optimize the cooling system to have the right fluid saturation temperature, depending on the evaporator's functioning temperature range. Depending on the application, enhancements can be provided through surface treatment [2-3]. Other applications under size-bounded configurations need to work in a confined boiling situation [4], which can be advantageous for a specific range of heat flux. The geometrical configuration is another aspect to study upfront to allow the most beneficial flowing condition, including the position of the condenser [5]. Thermal solutions aim to use the less fluid possible for the packaging of the cooling system, both for practical and economic reasons. Because most of the thermal solutions include an electrical factor, focus is shifted towards dielectric fluids. In particular, Novec 7000 fluid is used in this experimental study.

Nukiyama [6] in 1934 was the first to establish that a maximum heat flux existed for a given fluid to be able to evacuate all the heat created on the evaporator surface. Since then, other studies have been conducted further investigating pool boiling mechanisms and parameters. A summary of the most related research correlations has been redacted in **Table 1**, ordering the correlations at increasing heat flux. Han and Griffith [7] in 1964 established that bubble initiation in pool boiling was influenced by the temperature of the surrounding fluid and the surface condition. A thermal boundary layer model was proposed, combined with a critical wall superheat relation, but the authors admitted the complexity of the phenomenon and its intrinsic randomness, which makes difficult the interpretation of their results. Also, Hsu [8] proposed a simplified model to evaluate the size of the thermal boundary layer and the range of cavities which can become active nucleation sites. More than half a century later since Nukiyama [6], a lot more data has been gathered on boiling allowing a basic understanding of some of its phenomena, to create different models to characterize nucleate boiling and to predict critical heat fluxes. However more recently in 2017, Leong and Wong [9] realized a critical review of pool boiling of dielectric fluids and the authors affirm that these models

only have relative success. They also state that studies on boiling with dielectric fluids – which are highly wettable – need further investigation for more complete comparative studies.

Confined boiling represents a more specific segment of research on boiling, which has seen more interest in the more recent decades both for packaging reasons and its possible enhancement effects in certain situations. Bonjour [4] found that confinement could improve heat exchange for lower heat fluxes compared to pool boiling. He also identified three confined boiling regimes depending on the bubble sizes and shapes, which correspond generally to the observations of Yao and Chang [10], Xia et al. [11] and Rampisela [12]. These regimes are with increasing heat flux: the isolated bubble regime, the coalesced bubble regime and the partial dry-out regime (**Fig. 1**).

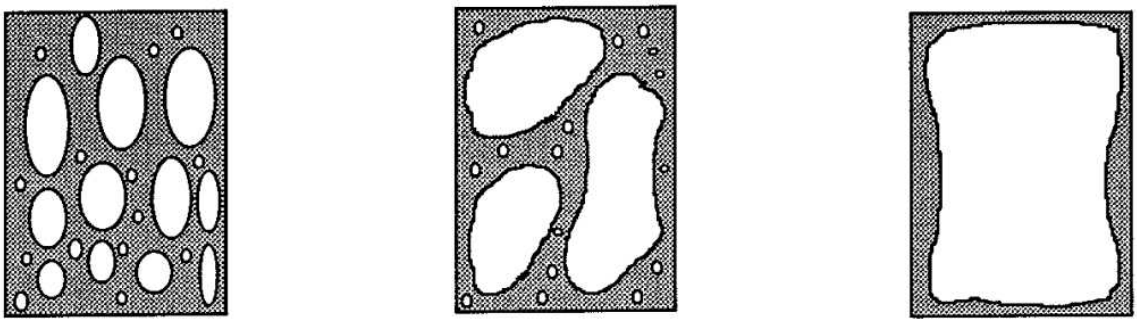

Figure 1 - Boiling regimes identified by Bonjour and Lallemand [47]: (a) isolated bubble, (b) coalesced bubble regime, (c) partial dryout regime

Ait-Ameur [13] o t state: a stationary upward flowing regime and a pulsed boiling regime. The latter takes place when vapor creation is more important than capillary and viscous effects, rendering the supply of fresh fluid impossible on the heated surface. Furthermore, he observed an enhancement of up to 600% of the heat exchange at high confinement for low heat fluxes. Both Bonjour [4] and Ait-Ameur [13] have additional data about the liquid-vapor phase ratio in a canal through hot wire anemometric measurements coupled with optical visualization with R-113 fluid. They both observe an increase in heat exchange for small canal widths at low heat flux compared to the free case, but their mass flow measurements are discordant. Bonjour's mass flow measurements [4] show that the reduction of canal width increases the fluid mass flow, leading to an increase of convective effects. Two additional phenomena were also reported to explain the increase in confined heat exchange. Firstly, the expansion of the interface surface between liquid and vapor phase and the wall: as bubbles are flattened, the liquid microlayer between the wall and the vapor is stretched. Secondly, because the bubbles are flattened, this

facilitates vapor to enter and activate other nucleation sites on the surface, further boosting phase change heat transfer. On the contrary Ait-Ameur's data [13] shows that the reduction of canal width decreases the average mass flow. At a higher canal width, he justifies the increase in fluid mass flow to viscous effects and pressure loss decreasing. Still, the author also measures an increase in confined heat exchange, but in this case it cannot be associated to an increase of convection. The author then proceeds to explain the confined heat exchange enhancement depending on the canal width:

- For canal widths larger than the capillary length, the increase in heat exchange comes from the convection improvement, as fluid mass flow increases
- For canal widths smaller than the capillary length, the superior heat exchange comes from an increase of the interface surface between liquid-vapor phase and the wall, plus an increase of nucleation because of bubble flattening

Both Bonjour [4] and Ait-Ameur [13] observe that the fluid mass flow always increases with heat flux independently of confinement. For the same canal width, the quantity of liquid-phase fluid in the canal is very sensitive to the heat flux, plus its presence remains substantial even near critical heat flux. Finally, Ait-Ameur [13] does not observe a significant influence of the heated surface width on heat exchange, but canal height is inversely proportional to the critical heat flux because of vapor accumulation in the channel. The lateral width of the canal also has a negligible effect on heat exchange, except for the critical heat flux which decreases up to 30%.

As shown in **Table 1** the literature is rich in correlations derived for specific systems, to identify the beginning or the transition between boiling regimes. The Zuber [14] analytical treatment considered the Taylor instability criterion for vapor columns formed by coalesced bubbles and defined critical heat flux as the heat flux at which the vapor–liquid interface becomes unstable. Bonjour and Lallemand [15] proposed their own correlation for critical heat flux for R-113 on a vertical confined copper plate. Monde et al. [16] proposed a correlation of critical heat flux based on their experimental study on a vertical channel with different fluids, its precision was of +/- 20% compared to their experimental data. Later Geisler and Bar-Cohen [17] complained that in the literature most fluids used are either water or R-113, which have very different properties compared to dielectric fluids which are often highly wettable. Several critical heat flux prediction correlations are based on Zuber's research [18], to then expand and adapt his correlation to a specific combination of fluid-wall

interaction. More recently, El-Genk and Pourghasemi [19] experimentally investigated boiling critical heat flux of Novec 7000 on rough copper surfaces, proposing several empirical correlations which are unfortunately very limited to their specific fluid and surface. In 2014, the literature review for boiling of Cheung at al. [20] establishes that not one single combination of empirical correlations has shown the propensity of providing satisfactory predictions in the literature. Since then, there has been a more recent study from Alsaati et al. [21] proposing a mechanistic model to predict CHF in a vertical confined gap. Although the proposed correlation takes into account the gap size, inclination and the fluid properties, it is based on other authors experimental data points which are obtained for the most part with different boundary conditions compared to the present study: for example, a copper heated plate instead of steel, different fluids and different inlet/outlet flowing conditions for the fluid.

Ref.	Author(s)	Configuration	Fluid	Correlation proposed	Equation N°
[22]	Incropera	Free convection on an upward horizontal plate	-	$Nu = 0.15\, Ra^{1/3}$	(1)
[23]	Suzsko & El-Genk	Free convection on upward horizontal plate	PF-5060	$q'' = 0.038\left(T_p - T_{sat}\right)^{1.2}$	(2)
[24]	El-Genk & M. Pourghasemi	Free convection on upward horizontal plate	Novec 7000	$q'' = 0.042\left(T_p - T_{sat}\right)^{1.2}$	(3)
[25]	Bahrami	Free convection on vertical plate	-	$Nu = 0.1\, Ra^{1/3}$	(4)
[26]	Churchill and Chu	Free convection on vertical plate	-	$Nu = \left\{0.825 + \frac{0.387\, Ra^{1/6}}{\left[1+\left(0.492/Pr\right)^{9/16}\right]^{8/27}}\right\}^2$	(5)
[27]	Gan	Convection for tall ventilation cavities	Air	$Nu = 0.135\left(Ra\left(\frac{H}{e}\right)^{3/2}\right)^{0.265}$	(6)

[28]	W. M. Rohsenow	A method of correlating heat transfer data for surface boiling of liquids	-	$q'' = \mu \Delta h_{lv} \left(\frac{1}{C_{sf}} \right)^{1/r} Pr^{-s/r} \left[\frac{c_p \left[T_p - T_{sat}(P) \right]}{\Delta h_{lv}} \right]^{1/r} \left[\frac{g(\rho_l - \rho_v)}{\sigma} \right]^{1/2}$ With r=0.33, s=1.7 and $C_{s,f}$ depending on the combination fluid/wall. For water and stainless steel $C_{s,f}$=0.015	(7)
[29]	Stephan and Abdelsalam	Natural convective boiling with horizontal copper/steel tubes	R-113	$q'' = \left\{ 1.1 \left[T_p - T_{sat}(P) \right] \right\}^{1/0.255}$	(8)
[30]	Forster and Zuber	Dynamics of vapor bubbles and boiling heat transfer, comparison from literature data of pool boiling	Water, n-pentane, ethanol, benzene	$h = \frac{0.00122 \, \Delta T_{sat}^{0.24} \, \Delta P_{sat}^{0.75} \, c_{p,l}^{0.49} \, \rho_l^{0.49} \, \lambda_l^{0.79}}{\sigma^{0.5} \, \Delta h_{lv}^{0.24} \, \mu_l^{0.29} \, \rho_v^{0.24}}$ avec $\Delta P_{sat} = P_{sat}(T_p) - P_{sat}(T_l)$	(9)
[31]	El-Genk	Boiling on upward horizontal copper surface	Novec 7000	$h = 2.23 \left(1 - 0.66 e^{-2.65 Z} \right)$	(10)
[32]	Bromley	Film boiling on a horizontal heated cylinder	-	$h = 0.62 \left[\frac{\lambda_v^3 g \rho_v (\rho_l - \rho_v) \Delta h_{lv}^{'}}{\mu_v (T_p - T_{sat}) L} \right]^{1/4}$	(11)

				where $\Delta h_{lv}^{'} = \Delta h_{lv}\left[1+\frac{0.4\,c_{p,v}\left(T_p - T_{sat}\right)}{\Delta h_{lv}}\right]$	
[33]	Chang	Film boiling on a large flat horizontal surface	-	$h = 0.43\left[\frac{\lambda_v^3 g\left(\rho_l - \rho_v\right)}{\mu_v a_0}\right]^{1/3}$ where $a_0 = \frac{k_v\left(T_p - T_{sat}\right)}{2\,\Delta h_{lv}\rho_v}$	(12)
[18]	Zuber	Pool boiling on large, thick, upward-facing horizontal plates	Water	$q_{CHF,Zuber}^{''} = 0.131\,\Delta h_{lv}\rho_v^{1/2}\left[\sigma g\left(\rho_l - \rho_v\right)\right]^{1/4}$	(13)
[16]	Monde et al.	Natural convective boiling at atmospheric pressure in vertical rectangular channels (copper heater)	Water, ethanol, R-113, benzene	$\frac{q_{CHF}^{''}}{q_{CHF,Zuber}^{''}} = \frac{1.221}{1 + 6.7\times10^{-4}\left(\frac{\rho_l}{\rho_v}\right)^{0.6}\left(H/e\right)}$	(14)
[31]	El-Genk and Pourghasemi	Saturation boiling on rough inclined copper surfaces	Novec 7000	$\frac{q_{CHF}^{''}(Ra,\theta)}{q_{CHF,Zuber}^{''}} = \frac{C_{CHF}(Ra,\theta)}{0.131}$ With :	(15)

				$C_{CHF}(Ra,\theta)=0.23\,Ra^{0.065}\left\{1-4.7\times10^{-7}\theta^{2.74}\right\}$	
[15]	Bonjour and Lallemand	Convective boiling in a vertical channel, height constant, e=[0.5;2.5]mm, pressure of [1;3]bar	R-113	$\frac{q''_{CHF}}{q''_{CHF,Zuber}}=\left[1+6.39\times10^{-5}\left(\frac{\rho_l}{\rho_v}\right)^{\Psi}\left(\frac{H}{e}\right)^{1.517}\right]^{-1}$ where $\Psi=1.343\,P_r^{0.252}$	(16)
[34]	Xia et al.	Convective boiling in vertical rectangular narrow channels, copper surfaces e=[0.8,5]mm and free case	R-113	$\frac{q''_{CHF}}{q''_{CHF,Zuber}}=\frac{1}{0.131\left(4.59+0.11\left(\frac{H}{e}\right)\right)}$	(17)

Table 1 – Overview of different correlations and configurations from the literature

Because of boiling's intrinsic unpredictability and its dependance on numerous parameters (as it depends on countless other variables such as surface condition [35-38], pressure [39-41], fluid nature [42-43], wettability [44-45], inclination [46-49]) it was necessary to carry a more specific experimental research based on the conditions and fluid of interest to isolate only a few significant variables.

The issue of this research is to identify the main effects of confinement in an original configuration comprising adjacent horizontal and vertical heated plates representing a 90° corner of a parallelepipedal heating element. The focus will be on heat transfer coefficients, wall superheats and critical heat flux. Also, the influence of heating on one plate to the other is studied: this is realized comparing the simultaneous heating of both plates to when heating only one of the pair. The understanding of these criterions will allow an optimization path for the design of cooling systems based on this technology.

Tests have been conducted up to the critical heat flux to observe its occurrence, although for practical applications film boiling regime is to generally be avoided. Film boiling could be observed both in a quantitative way through the thermocouples' measurements and in a more direct and qualitative way through simple visual observation. The details of the testbench functioning and design are given in the next section, explaining in what way the testbench is original and represents a new configuration compared to the literature. In this experimental research, all the measurements are taken at the middle of the heated plates. Finally, boiling regimes and a stream map are characterized.

1 - Material and methods

1.1 - Description of experimental apparatus

A completely original testbench has been designed to regulate some input parameters such as heat flux, confinement, condenser's temperature and coolant mass flow. In addition, the setup allows to measure the pressure inside and the temperatures at different crucial locations in the system. 3M Novec 7000 is the dielectric fluid used for the immersion boiling testing, which has a 34°C saturation temperature at atmospheric pressure [50].

In **Fig. 2** and **Fig. 3**, the main components of the testbench are showed. The heating is provided by two Thermocoax SEA 10/75 heating elements for each heated plate. These plates are at a 90° angle from each other, between them there is a Deltherm thermal insulator piece ($\lambda_{Deltherm}$=0.25 W/m.K). This allows to heat the plates either simultaneously or separately, reducing the conductive heat exchange between them. The Thermocoax elements are 1mm diameter electric cables heated through Joule effect, delivering each up to 250W on 75 mm of the total length of the cable. Because they are so thin, they can bend several times within a 2mm bend radius. This allows a homogeneous distribution of heat flux in the copper plate: thermal simulation shows that for 20 W/cm² injected electric power, there is a conductive heat flux spread of 0.05 W/cm² on the plate. They are inserted in a 1.2mm deep groove on the sides of the 10mm thick copper plates (64x40mm²). The groove was previously machined to distribute the heat in the most homogeneous way.

The heat is then transferred from the copper plates to inox 316L steel plates (6mm thick and 64x40mm² surfaces) through some thermal paste to limit thermal contact resistance. The other side of the steel plates is in contact with the dielectric fluid, where the boiling takes place. Deltherm thermal insulator surrounds both the copper and steel plates all around except the boiling surfaces, granting low heat flux losses on the sides and behind the plates. This way, most of the heat created from the Thermocoax is conveyed to the boiling surface.

Once these different components are assembled, they create a unique solid piece that constitutes the heating element of the system, as shown in **Fig. 2**. This solution with two consecutive heating plates of different materials was chosen to first homogenize the heat flux coming from the electric cable in the copper plate (which has high conductive properties), plus allow a temperature gradient near the surface of the steel plate (which has lower conductive properties) due to local boiling effects, in order to measure heat flux.

The heating elements are completely immerged inside the fluid, which occupies the whole setup. There are no inlets or outlets, just the fluid that flows up and down depending on temperature gradients for convection and density difference for phase change. The L-shape design for the heating element has been chosen to represent a corner of a parallelepiped heating element.

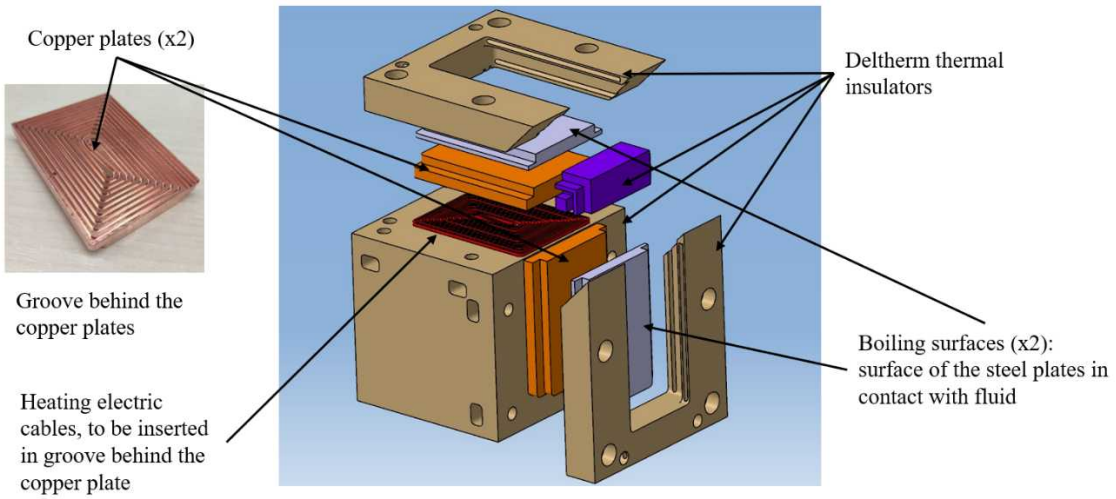

Figure 2 - Heating element assembly CAD schematic

A 2D schematic section of the most important components of the whole experimental device is shown in **Fig. 3**. The assembled heating element can be moved closer or farther from the glass wall through a 50mm long micrometer screw, which allows to regulate the confinement e in the canal in front of the vertical plate. The assembled heating element is mounted on two cylindrical rails to guide its movement.

A copper condenser with aluminum fins is situated 5 mm on top of the horizontal heating plate. The condenser has been intentionally oversized so that its heat exchange capabilities are enough for higher power tests (especially at or near film boiling testing). On the bottom of the system, a conduit connects the fluid inside the testbench to an expansion tank to help controlling the pressure at 1 atm while boiling takes place.

A wide glass window is installed in front of the vertical plate to monitor the system at any time. The transparent glass also represents the confining wall. Two other glass windows are situated on the sides, to either light the surface or to observe the boiling surface at a perpendicular angle.

Supplementary schematic material of the testbench - such as different views of the elements, the temperature measurement locations and fluid circulation – is presented in the Annex at the end of the article.

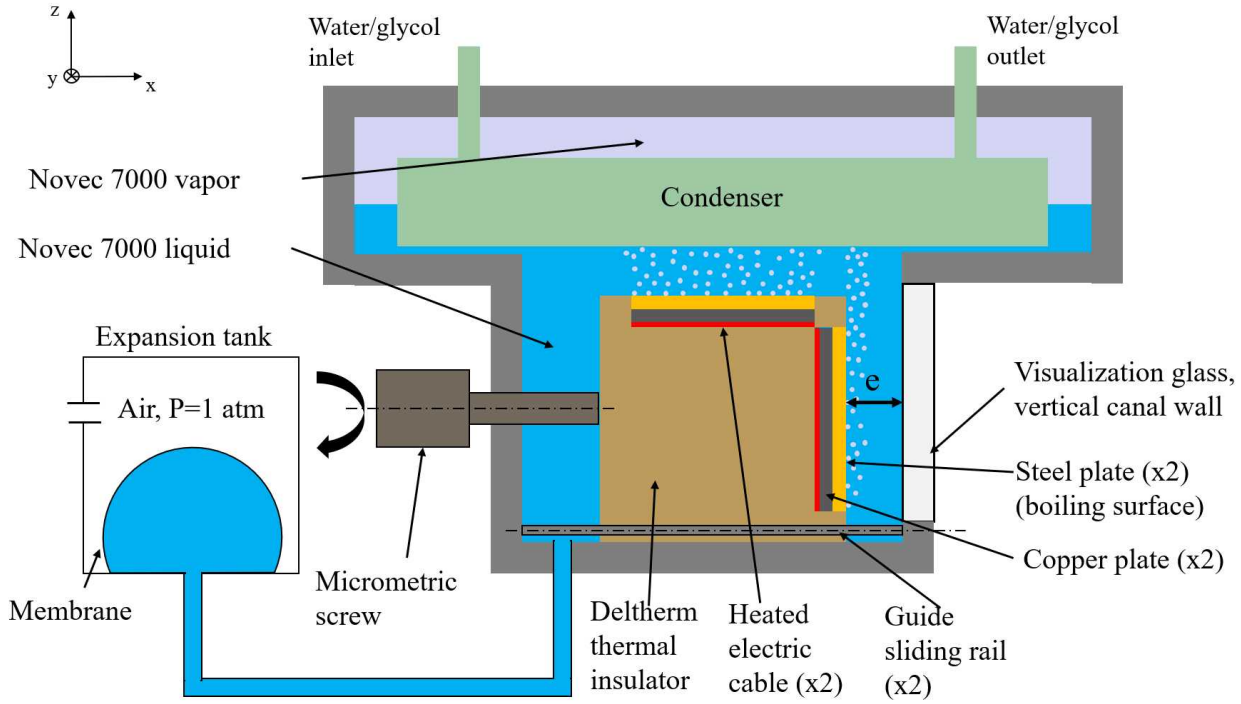

Figure 3 - 2D schematic plan of the main setup components

1.2 – Measurements

The main measurements inside the testbench are the temperatures, which are taken through K-type thermocouples of 0.5mm diameter. These thermocouples are situated at the middle of the heated plates at different depths, plus another thermocouple in front of the plate immerged in the fluid, as is explained in more detail in section **1.3**.

The thermocouples in both the vertical and horizontal steel plates are placed in depth below the surface to avoid interfering with boiling. Another thermocouple is placed inside the copper plate, near the heating element, in order to evaluate temperature at the hottest position of the system, to never exceed $T_{max} = 200\,°C$. The thermocouples' temperature accuracy is taken as 0.12 °C. Further details on their position and use to determine heat flux and heat transfer coefficients are given in section **1.3**.

A schematic representation of the whole setup is given in **Fig. 4**.

All the thermocouples are connected to a Keysight 34980A acquisition center, passing through a Keysight 34921A isothermal cold box to measure the cold junction temperature with better accuracy.

Confinement is measured through the micrometric screw which has a resolution of 0.01 mm and an accuracy of ±0.003mm. This allows to control the confinement value e of the vertical heated plate in a range of 0.5 mm< e <15 mm. This corresponds to a Bond number between $Bo = [0{,}27\,;\,244]$ where :

$$Bo = \frac{(\rho_l - \rho_v)\, g\, e^2}{\sigma} \qquad (18)$$

where σ is the surface tension of the fluid.

Pressure is measured with a Gems absolute pressure sensor, working between 0 and 6 bars with a precision of 0.25%. It is screwed in a hole in the top lid of the system. Furthermore, the pressure is kept near atmospheric pressure with an expansion tank. However, because of the expansion tank membrane stiffness, the pressure varies slightly from 1 bar to 1.2 bar when the highest heat flux is applied.

The temperature setpoint of the water/glycol mix circulating in the condenser is controlled by a Huber Unichiller P025-H unit and its mass flow is regulated through a Belimo LR24A electric valve and a IFM SM7000 inductive flow meter. The flowrate in the condenser is set to 7.4L/min for all measurements, which ensures a condenser inlet/outlet average temperature difference of 0.5 °C at the highest heat flux.

The Thermocoax heating elements are connected to two 80V-15A BK Precision 9115 power supplies, which provide the electric current necessary for the Joule effect.

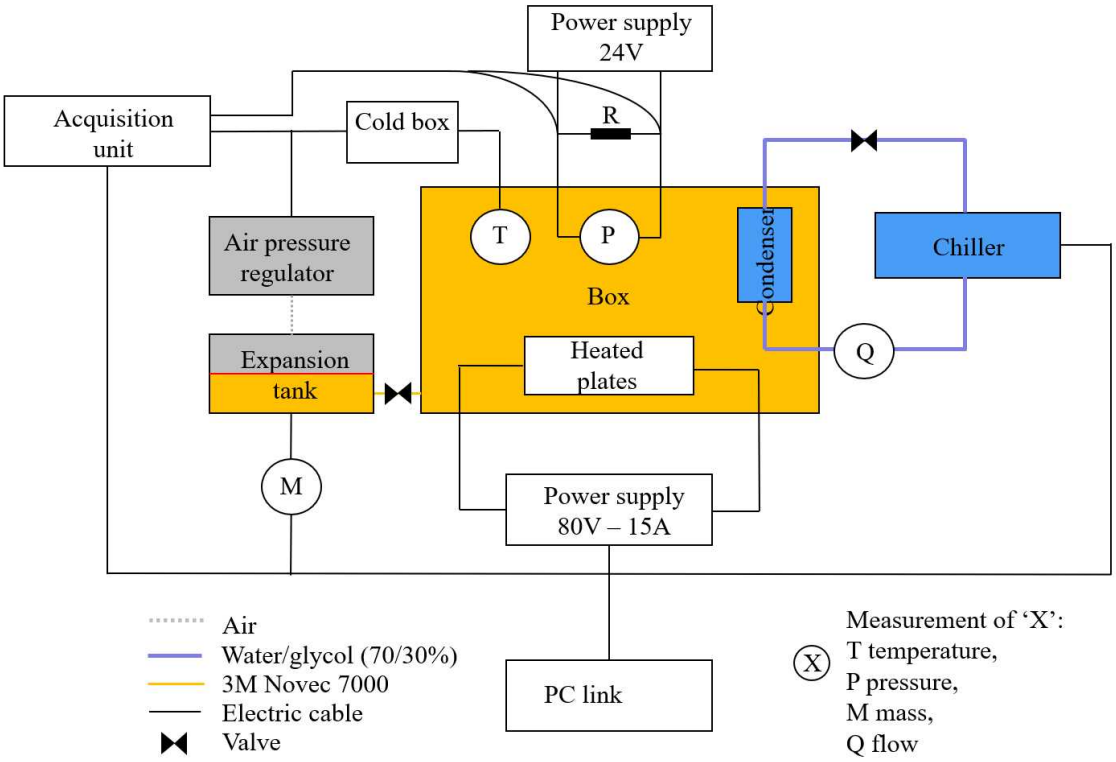

Figure 4 - Schematics of the testbench components

1.3 – Data reduction

Thermocouples are used to measure both the temperature and the heat flux in the middle of the heated plates. For this study, only the thermocouples in the central position of the heated plates are used: their location is shown in the Annex. On each steel plate, a thermocouple is found at a first depth e_1=0.7 mm from the surface, the other is at a distance e_2=2.3 mm deeper. There is also a third thermocouple T_3 at 11mm from the boiling surface, at the middle of the copper heated plate.

A schematic of three thermocouples at three different depths is given at **Fig. 5.**

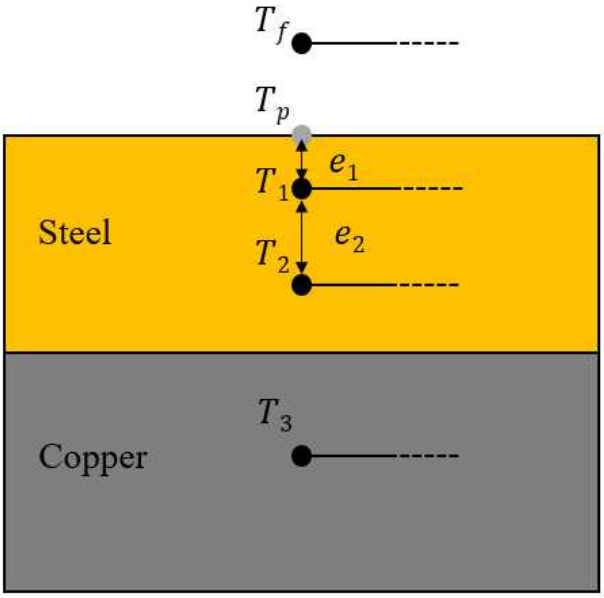

Figure 5 - Schematic of thermocouples at different depths of the heated plates

T_3 is the only thermocouple inside the copper plate, used to check the maximum temperature near the electrical cable. T_f represents the thermocouple measuring the fluid temperature in front of the heated steel plate, at an approximate distance of 2mm from the boiling surface. Only when the canal width in front of the vertical plate is less than 2mm, the T_f thermocouple is pushed closer to the boiling surface at a distance equal to the confinement. The surface temperature T_p is obtained from the T_1 and T_2 thermocouples inside the steel plate, through the thermal/electrical resistance equivalence. Here:

$$T_p = T_1 - R_{th,1} q'' S \qquad (19) \qquad \text{and} \qquad q'' S = \frac{T_2 - T_1}{R_{th,2}} \qquad (20)$$

Where T_p is the temperature at the boiling surface, S is the area of the boiling surface, q'' is the surface heat flux and $R_{th,1}$ and $R_{th,2}$ are the thermal resistances on the depths e_1 and e_2.

Under the assumption that the heat flux is the same between T_2-T_1 and T_1-T_p:

$$T_p = T_1 - \frac{e_1}{e_2}(T_2 - T_1) \qquad (21)$$

Concerning the uncertainties of these variables, a study has been realized. Considering that $u(e_1)=u(e_2)=u(e)$=0.1 mm and $u(T_1)=u(T_2)=u(T)$=0.2 °C (although the temperature accuracy is of 0.12°C, a higher value is chosen to account for thermal contact resistance), after

development and removing the uncertainty of surface dimensions as it negligible compared to other terms, the surface temperature relative uncertainty is equal to:

$$u(T_p)=\sqrt{u(T^2)+\sqrt{\left(\sqrt{\left(\frac{\sqrt{2}u(T)}{T_1-T_2}\right)^2+\left(\sqrt{\left(\frac{u(e_2)}{e_2}\right)^2+\left(\frac{u(\lambda)}{\lambda}\right)^2}\right)^2}\right)^2+\left(\sqrt{\left(\frac{u(e_1)}{e_1}\right)^2+\left(\frac{u(\lambda)}{\lambda}\right)^2}\right)^2}}$$

(22)

In the same way, after development it is also possible to determine the heat flux and the heat transfer uncertainties:

$$\frac{u(q'')}{q''}=\sqrt{\left(\frac{\sqrt{2}u(T)}{T_1-T_2}\right)^2+\left(\sqrt{\left(\frac{u(e_2)}{e_2}\right)^2+\left(\frac{u(\lambda)}{\lambda}\right)^2}\right)^2} \quad (23)$$

To verify that the monodirectional direction of the heat flux is acceptable, a 3D model has been studied with a thermal simulation software. The model includes the steel and copper plates, plus the electrical resistance and the Deltherm thermal insulator on the sides. All the components are immerged in the fluid. Contact thermal resistance were added between the components. Different simulations were run, using different heat transfer coefficients depending on the heat flux applied. The heat transfer coefficients were chosen based on Novec 7000 literature and the first experimental data obtained with the testbench. The losses were in a range between 5-10% of total heat flux, depending on the power applied and the heat transfer coefficient chosen. This is considered acceptable for using the thermal resistance to estimate the surface temperature.

A verification of injected power and measured heat flux is realized with the testbench. At the highest heat flux, the electric power injected is 500W. The power measured through the thermocouples in the middle of the heated plates is often close to the injected power with less than 10% thermal losses. In every figure shown in the present study, the heat flux shown is the one measured through the thermocouples in the middle of the plate.

The heat transfer coefficient *h* is obtained through Newton's formula for heat flux, using the temperature in the fluid and the temperature at the surface:

$$h=\frac{q''}{T_p-T_f} \quad (24)$$

Its uncertainty is equal to:

$$\frac{u(h)}{h}=\sqrt{\left(\sqrt{\left(\frac{\sqrt{2}u(T)}{T_1-T_2}\right)^2+\left(\sqrt{\left(\frac{u(e_2)}{e_2}\right)^2+\left(\frac{u(\lambda)}{\lambda}\right)^2}\right)^2}\right)^2+\left(\frac{\sqrt{2}u(T)}{T_S-T_f}\right)^2} \quad (25)$$

Finally, the superheat is determined comparing the surface temperature T_p to the saturation temperature. Saturation temperature is adjusted at any time depending on the measured system pressure. The detailed expression are as follows:

$$\Delta T = T_p - T_{sat}(P) \quad (26)$$

And: $$T_{sat}(P) = 26.924 \ln(P) - 2.61 \quad (27)$$

Eq. 27 was obtained interpolating data points of Rausch et al. [51] study on HFE fluid properties. It is to be used with the following units: temperature in K and the pressure in Pa.

1.4 – Experimental procedure

1.4.1 – Filling, filtration and draining of testbench

All the experimental tests are obtained following a specific procedure. First, a vacuum pump is used to remove the air from the testbench. This helps to avoid embryos of air sticking in the tiny cavities all along the boiling surface. Otherwise, the air embryos would trigger the onset of boiling sooner. Also, the presence of air would change the fluid properties. The fluid is degassed by heating it (>100°C) and releasing for a few seconds from the top vapor outlet. Then it is possible to fill the bench with filtrated dielectric fluid from a reservoir in liquid phase. A difference in pressure is created between the heated reservoir and the testbench to fill up. As the reservoir is placed on a balance, the mass of transferred fluid is also measured.

Once testing is finished, the setup is drained and the dielectric fluid is filtered at the same time. To do so, the testbench is connected to a refrigerant recovery unit through a dehydrating filter. The condenser inside the testbench is brought at 45°C, which increases the system pressure and evaporates most of the fluid. At the same time all the pipework and the recovery unit are voided with the vacuum pump. Finally, an outlet valve on the roof of the testbench is used to extract the fluid vapors which get through the dehydrating filter, then the recovery unit and finally the storage tank.

1.4.2 – Testing procedure

First, the condenser is set at the desired water/glycol temperature through the chiller. Once the temperature set by the chiller is stabilized, the rest of the test can be realized, namely the heating in the plates.

Because the experimental testbench can observe the effect of boiling hysteresis, most results are obtained at decreasing heat flux. This is common in boiling literature.

Indeed, when no nucleation sites are active, a higher wall superheat is required to start the nucleation. For the same wall temperature, the heat flux can undergo a hysteresis: lower heat flux is needed if nucleation has previously been activated.

It is possible to appreciate this phenomenon in a qualitative manner through a couple of snapshots shown in **Fig. 6**. The same heat flux is applied to the vertical plate in the increasing **(Fig. 6.a)** then decreasing **(Fig. 6.b)** heat flux situation.

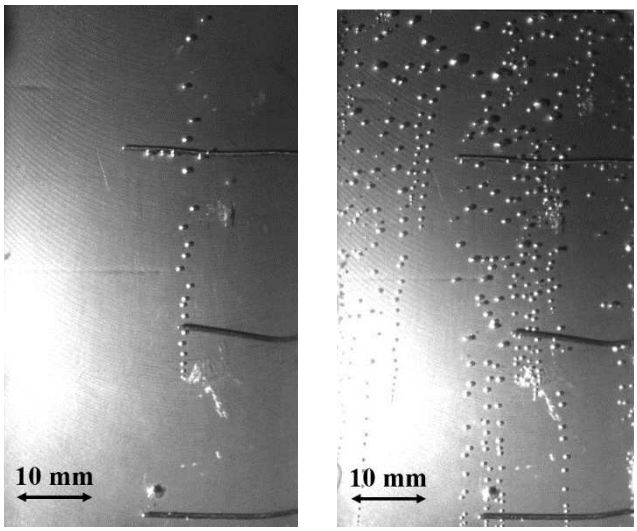

At decreasing heat flux an important number of previously activated nucleation sites are still active. For the increasing heat flux, heat flux is only enough for the activation of one nucleation site.

Given the high number of bubbles at the decreasing heat flux, the heat transfer coefficients are improved by the bubbly flow, which allows lower superheats.

Measuring at decreasing heat flux pre-activates the nucleation sites on the whole surface. This way the boiling hysteresis at low heat flux is avoided. To do so, the heat flux is directly increased to the highest value to be studied. Then it is decreased at the different values desired, waiting for the steady-state regime between each of them. Steady-state regime is considered reached when all the thermocouples' measurements do not vary more than 0.5 °C over a 5 minute period at least when near partial dryout points, an accuracy of 0.2°C can be used for other cases. In general, it could be achieved in 25 minutes for higher heat flux and up to 40 minutes for the very low heat flux.

1.4.3 – Repeatability test

A repeatability test has been realized at different times. The average temperature measurements on the plates are repeatable. More precisely focusing on the heat flux, the worse accuracy is at low heat flux where the points are within a 20% relative error. For medium and high heat flux, the relative error is less than 5%.
Concerning the temperatures, the worse relative error between the repeatability tests is at medium heat flux at with a maximum gap of 4°C. All other points are within a 1°C temperature difference.

The variation of mass fluid inside the system has also been considered. It is found to be the most important criterion when reproducing the same tests with different fillings. Because it is a closed system the fluid mass introduced inside influences the system pressure, therefore the saturation temperature and the boiling heat exchange.

Therefore, through all the data comparisons presented in the rest of this article, they are obtained on one single filling of the experimental bench. This guarantees the same mass fluid inside the system for the same testing.

2. Results and discussions

2.1 – Free boiling on horizontal plate

A free boiling study for the horizontal plate has been carried out to validate the experimental testbench and compare its results to the boiling literature, which is for the most part dedicated to horizontal upward heated plates. This both constitutes a baseline test to validate the apparatus and allows a comparison with the vertical configuration for the next section.

For this test, the condenser was set at 32°C and the wall superheats are calculated using the saturation temperature adjusted at the measured pressure for each data point. The data points are measured at decreasing heat flux. The resulting boiling curve is shown in **Fig. 7**.

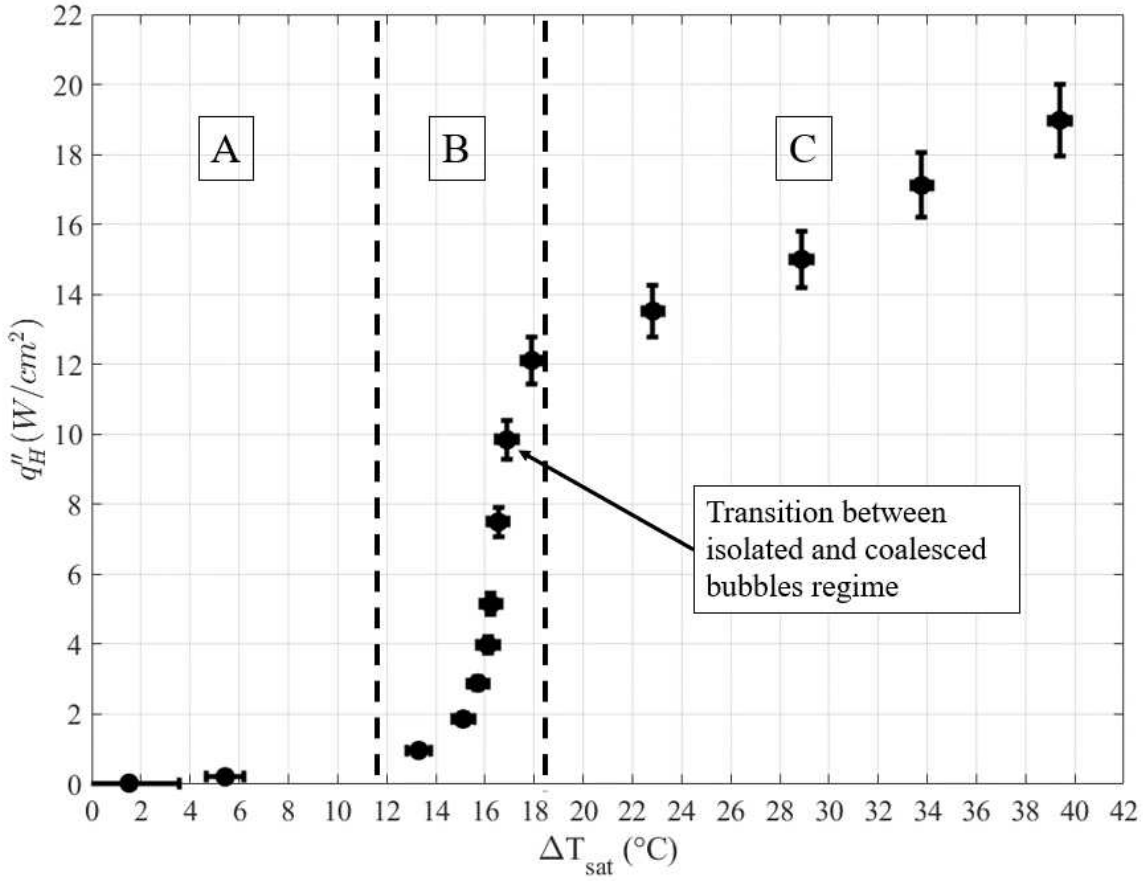

Figure 7 - Free boiling curve for the horizontal surface

3 main boiling regimes are detectable in **Fig. 7**. Although no visual observation could be made because of the position of the horizontal heated plate inside the system, based on the difference in the slope of the data points and linking it to the literature it is possible to theorize the difference in the regimes observed. The literature in question is Gaertner's photographic study [52] and Zuber's proposition [53] on the transition between isolated bubbles and the fully developed boiling on a horizontal heated plate.

In **Fig. 7**, region A corresponds to the convection prevailing regime. At very low heat flux, it is predictable that the heat flux released from the heated plate is still insufficient to supply the liquid-vapor phase change for most of the vapor embryos on the surface. Further proof of the predominance of convection in this regime, is the gap in measured heat flux between the second and third point of the series. The explanation is that at very low heat flux, most nucleation sites fade out thus decreasing the heat transfer coefficient on the heated surface,

drawing near convection. Therefore, a greater portion of heat flux is lost to the conduction to the sides of the plate instead of going through it.

Region B of **Fig. 7** corresponds to the boiling regime. In this regime, there are several progressive transitions. The low heat flux zone of B corresponds to the isolated bubble boiling regime, where most nucleation sites are still sustained (at decreasing heat flux) and drastically increase the heat transfer rate on the surface through a mix of enhanced convection by bubbly flow and phase change. In this region, the heat flux density can be multiplied tenfold but the wall superheat only increases by 4°C. This is because most of the new heat flux introduced in the system is absorbed by the latent heat to supply the vapor phase change, which is not yet covering the whole surface. This zone typically represents the best regime for working cooling applications, as the wall superheat is contained in a narrow range. As is marked in **Fig. 7**, there is a point that marks the shift towards fully developed boiling, from where the slope starts to decrease again. This can be interpreted for the plate being completely covered in active nucleation sites, which allows the development of a different flow configuration at the global level in front of the heated plate. At higher heat flux, jets of vapor begin to form. These can combine to form small vapor mushrooms.

Zuber [53] proposed a correlation for the transition between the isolated boiling sub-regime to the fully developed boiling sub-regime:

$$q_{trans}=0.8\,\rho_v\,\Delta h_{l,v}\left[g\sigma/\left(\rho_l-\rho_v\right)\right]^{1/4} \qquad (28)$$

Where ρ_v and ρ_l are the vapor and liquid density, $\Delta h_{l,v}$ is the latent heat of vaporization, g is the constant of gravity acceleration and σ is the surface tension. With **Eq. 28** applied to Novec 7000 properties on a horizontal surface, the predicted transition heat flux is q_{trans}=10 W/cm². This agrees well to the change of slope observed in the boiling curve at this transition point.

Finally, region C in **Fig. 7** presents a different slope indicating a much slower increase of heat transfer coefficient for higher heat flux. This time, the wall superheat increases at a significant faster rate compared to the heat flux. This suggests the approaching of the film boiling regime, where the whole surface can gradually become covered in a thin layer of vapor. The vapor layer, because of its poor thermal properties, acts as insulation. The shift towards film boiling is also progressive, passing through a partial dry out phase where only smaller zones of the surface are intermittently covered in vapor.

Zuber's [18] correlation for critical heat flux is particularly adapted to the present study, as it is proposed for a horizontal upward heated plate. With Zuber's correlation of **Eq. 13** in **Table 1**, the predicted value of CHF is $q_{Zuber,CHF}$=19 W/cm². This agrees well with current experimental data, as suggests the high wall superheat increases measured near this heat flux.

A comparison of the same experimental data to convection and boiling heat transfer correlations is shown in **Fig. 8**. A logarithmic scale has been applied to better visualize the differences both at low and higher heat flux.

The correlations have been applied with the experimental measurements of the temperatures

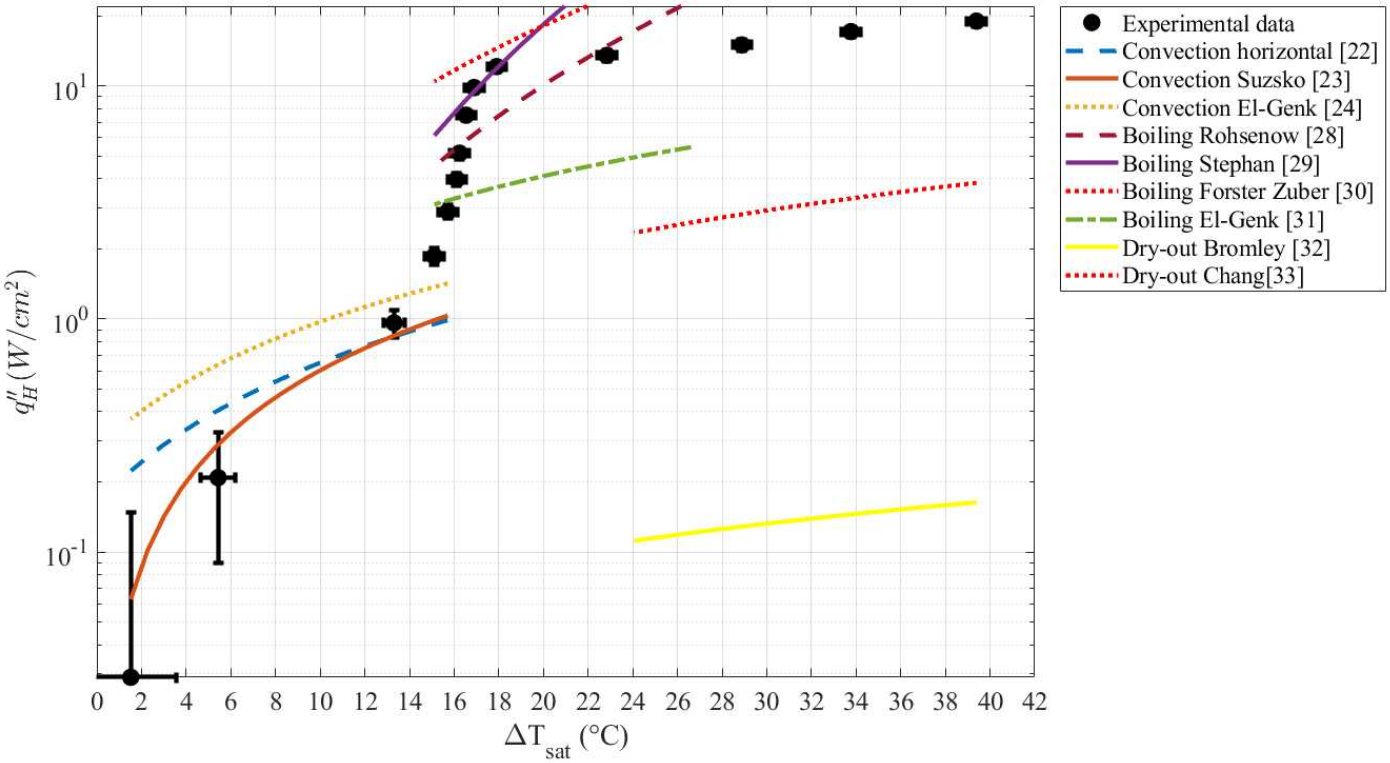

Figure 8 - Free boiling curve on horizontal plate with literature comparison

to determine the heat flux, which is then shown in **Fig. 8**. At low heat flux - up to 1,5 W/cm² - convection correlations are used, to overlap the convection prevailing regime A of **Fig. 7**. The first correlation for horizontal convection correlation (see **Eq. 1** from Incropera [22] in **Table 1)** is the most widely used in the literature for upward horizontal plates for which the Rayleigh number is at least $1x10^7<Ra<1x10^{11}$, in this case Rayleigh number is $Ra=1x10^{10}$. The Suzsko correlation of **Eq. 2** [23] is based on experimental results of PF-5060 dielectric fluid on a small copper surface, while the El-Genk **Eq. 3** [24] is based on experimental data with Novec 7000 on a small copper surface. As can be seen in **Fig. 8**, for heat fluxes of less than 0,3 W/cm² most correlations predict a lower wall superheat compared to the measured

one. This can be explained with the better heat transfer rate of copper compared to the steel surface of the present study. They do agree with current experimental data around 1 W/cm², then start to predict higher wall superheats at higher heat flux. The lower measured wall temperatures for q'>1 W/cm² are explained by the phase change phenomena present here, which increase the heat transfer rate.

For the developed boiling correlations, the Rohsenow [28] (**Eq. 7**) and Forster-Zuber [30] (**Eq. 9**) especially predict lower wall superheats compared to experimental data. The Stephan-Abdelsalam [29] (**Eq. 8**) is the closest to experimental data, especially up to the developed boiling regime at 10 W/cm², but for higher heat flux it also predicts lower wall superheats. Once again, the plate being made of steel, the heat exchange can be decreased by its lower conductivity. Moreover, these correlations were developed especially for developed boiling regime and not partial dry-out. This is contradicted by the El-Genk [31] correlation (**Eq. 10**) which is also found for boiling with Novec 7000, but with a copper heated plate of 10x10 mm² and at 0,85 bar. The lower saturation condition coupled with the smaller size of the heated plate promotes the appearance of film boiling sooner, thus lowering its heat transfer coefficient and increasing the wall superheat. This explains why our experimental data provides lower wall superheat compared to that of El-Genk.

Finally, the correlations for film boiling from Bromley [32] **(Eq. 11)** and Chang [33] **(Eq. 12)** predict very small values of heat flux. This is because their correlation is especially fitted for stable film boiling regime, where a constant layer of vapor covers the heated surface. This is not the case here, as during partial dry-out there is intermittent passing between liquid and vapor phase on the heated plate.

2.2 – Free boiling on vertical plate

The free pool boiling case on the vertical plate is realized setting the canal width at 15mm. The vertical heated surface is heated on its own for these tests. To justify that 15mm is enough to consider a free boiling configuration, the capillary length L_{cap} can be calculated. This value gives the minimum distance between the walls before confinement effects can be observed in a canal. It is not a foolproof quantity, but it gives an appreciation of the order of magnitude of this conceptual distance.

$$L_{cap} = \sqrt{\frac{\sigma}{g(\rho_l - \rho_v)}} \tag{29}$$

Different authors have discussed about correlations starting from L_{cap} to obtain the closest to the real value of the transition between microscale (where gravitational forces can be neglected) and macroscale (surface tension effects can be neglected compared to gravitation). Layssac [54] realized a scientific review of the different ways of calculating the capillary length, depending on the author's definition. He found that the correlations of the criterion for the transition distance from macroscale to microscale range from $d_{tr}=0.134\,L_{cap}$ to $d_{tr}=2\,\pi\,L_{cap}$. For Novec 7000, L_{cap}=0.9 mm. It is then possible to safely assume that a 15mm gap between the walls is enough to consider the system in the free configuration case. Indeed, in the worst case $d_{tr}=2\,\pi\,L_{cap}=5.7\,mm$ which is still much smaller than our 15mm distance.

An example of a typical result produced by the experimental procedure is given in **Fig. 9**. The error bars show the uncertainties calculated for each point. It represents a boiling curve as in most boiling literature, with wall superheat on the x-axis and surface heat flux on the y-axis.

In **Fig. 9.A**, it is possible to see that a considerable number of bubbles is still active even at low heat flux. As explained in the previous chapter, all the points of the boiling curves are obtained at decreasing heat flux. This is the reason why even at the lowest heat flux there are still some nucleation sites active, as they were activated sooner at a higher heat flux. At very low heat flux, convection still plays an important role. Therefore, this regime can be defined as 'enhanced convection', as the limited nucleation still creates a bubbly flow improving the heat transfer coefficient compared to convection alone. Compared to the horizontal plate, the bubbly flow created from the few nucleation sites still active further enhances heat transfer coefficient: this is because of the vertical configuration. Indeed, because of gravity the bubbles travel along all the surface and improve the mixing of hot and cold fluid in front of it. On the other hand, for the horizontal plate, when the bubbles are created, they instantly ascend interacting a lot less with the adjacent surface.

For a heat flux of more than 2 W/cm² the density of active nucleation sites is increased as they are distributed more evenly across the heated surface. Although boiling is developed at this stage, the bubbles have little to no interaction with each other. This corresponds to the

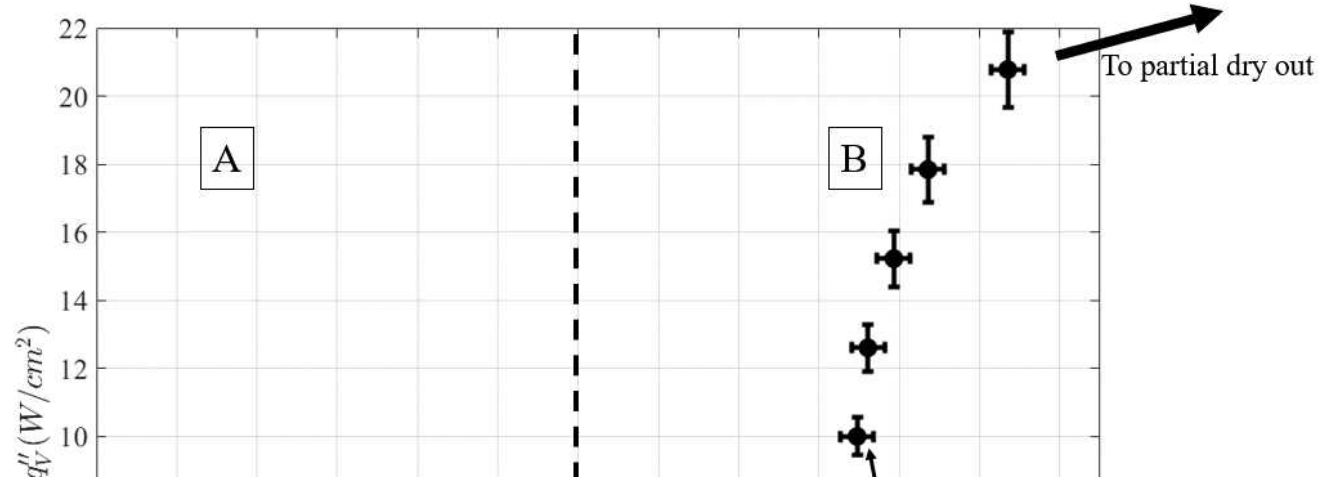

'isolated bubble regime' as seen in **Fig. 9.B1**. Moreover, an inflexion point is present around 2 W/cm², as the data slope changes. This represents the point where boiling starts to prevail on convection heat exchange.

At around 10 W/cm² coalescence appears in **Fig. 9.B2** and another inflexion point in the boiling curve is observed in the boiling curve. This represents the point where coalesced boiling occurs, further improving heat exchange and entering a new regime. This happens when vapor creation is faster than its ejection from the boiling surface.

Film boiling is typically observed as an asymptote, with very high increases of wall superheat with a small increase of heat flux. In the free configuration, the testbench heat flux was not enough to observe critical heat flux. However, at the highest heat flux the slope of the boiling curve was strongly decreasing, meaning that film boiling was approaching.

In **Fig. 10** the same boiling curve is compared to the literature to validate the reference data for the free configuration with both convection correlations at low heat flux – Bahrami [25] (**Eq. 4**), Churchill and Chu [26] (**Eq. 5**), Gan [27] (**Eq. 6**) - and pool boiling correlations at higher heat flux -Rohsenow[28] (**Eq. 7**), Stephan and Abdelsalam [29] (**Eq. 8**) and Forster and Zuber [30] (**Eq. 9**). A logarithmic scale is applied to facilitate the comparison for both low and high heat flux.

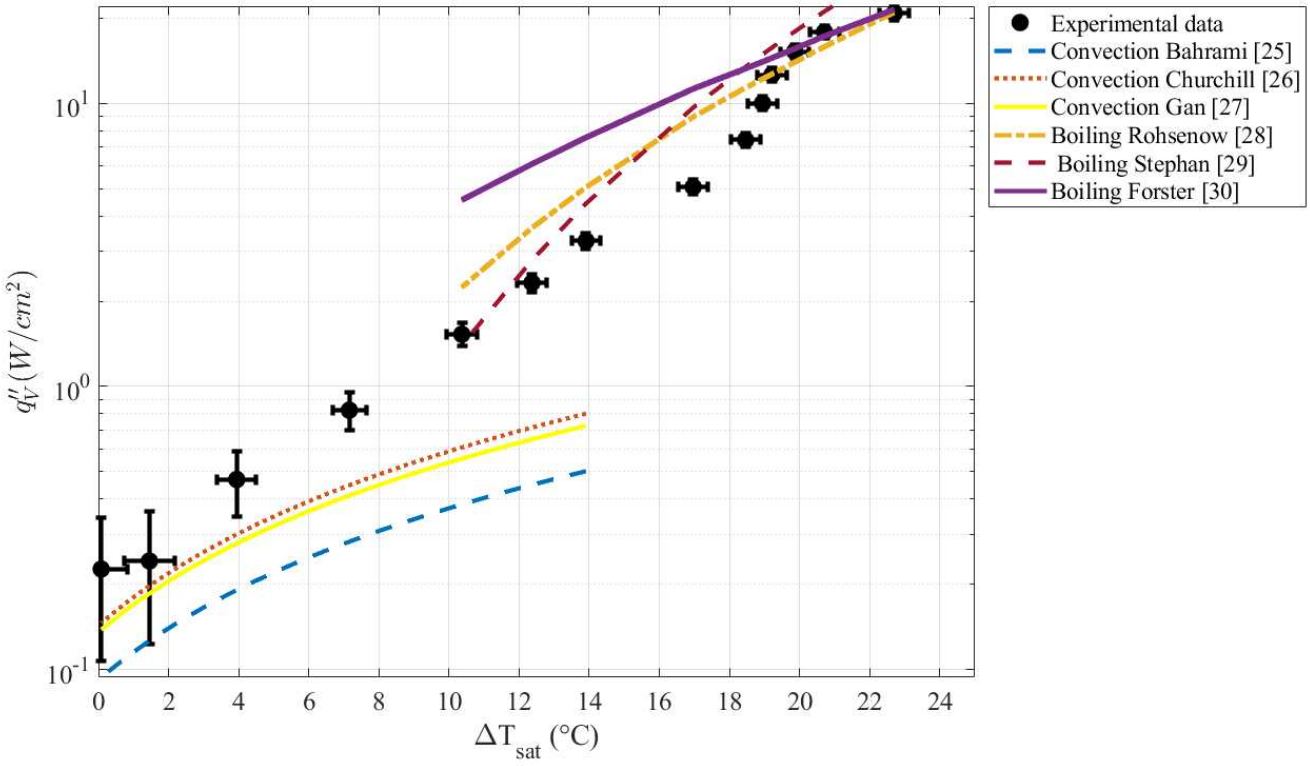

Fig. 10 – Reference boiling curve with literature comparison for validation

In **Fig. 10**, the points at low heat flux are compared to a correlation of convection in front of a vertical plate from Bahrami [25], Churchill and Chu [26] and from Gan [27]. For heat flux lower than 1 W/cm², both convection correlations produce quite close wall superheats to present experimental data. Up to 0.5W/cm², convection seems to be the biggest contributor to the heat exchange. For heat flux higher than 1 W/cm², the gap between convection and experimental data grows, meaning the slight bubbly flow has an increasingly important role in increasing the heat exchange coefficient. The difference between the current experimental data and the convection correlations is bigger for the vertical plate compared to the horizontal plate: this is once again because of the vertical configuration and its particular enhanced convection regime, which allows the bubbly flow to interact more with the heated plate at low heat flux.

The points at high heat flux are compared to three correlations from boiling literature. For the Rohsenow boiling correlation, the coefficient representing the couple of fluid/wall interaction between Novec 7000 and stainless steel could not be found. It was adjusted as advised by Van Carey [55] to better follow experimental data for refrigerants. The coefficient of **Eq. 7** from **Table 1** is taken at C_{sf}=0.005. Both Rohsenow [28] and Abdelsalam [29] correlations predict wall superheats that are always less than 2 °C away from present experimental data.

The Forster and Zuber correlation [30] predicts lower values of wall superheat than present data with the biggest difference in the isolated bubble regime. At higher heat flux it correlates more closely with present data, which can be expected as this correlation is mostly true for fully developed boiling regime at higher heat flux.

2.3 – Enhanced convection regime on vertical plate

7 configurations have been studied with different vertical canal widths, from the free case to the most confined one being at e = 0.5 mm. In the present section, the heat flux on the vertical plate is shown between 0 and 3.5 W/cm², the horizontal plate was not heated. The condenser water/glycol mixture input was set at 32 °C with a flow rate of 7.4 L/min. Only the vertical plate was heated for this comparison.

The results can be seen in **Fig. 11.A**, where a clear order is observed for each heat flux: the higher the confinement, i.e. the smaller the canal width, the lower the wall superheats.

The free configuration consistently produces the highest superheats. Also, the free configuration case is very close to when e = 2 mm for q''>2 W/cm². This validates our

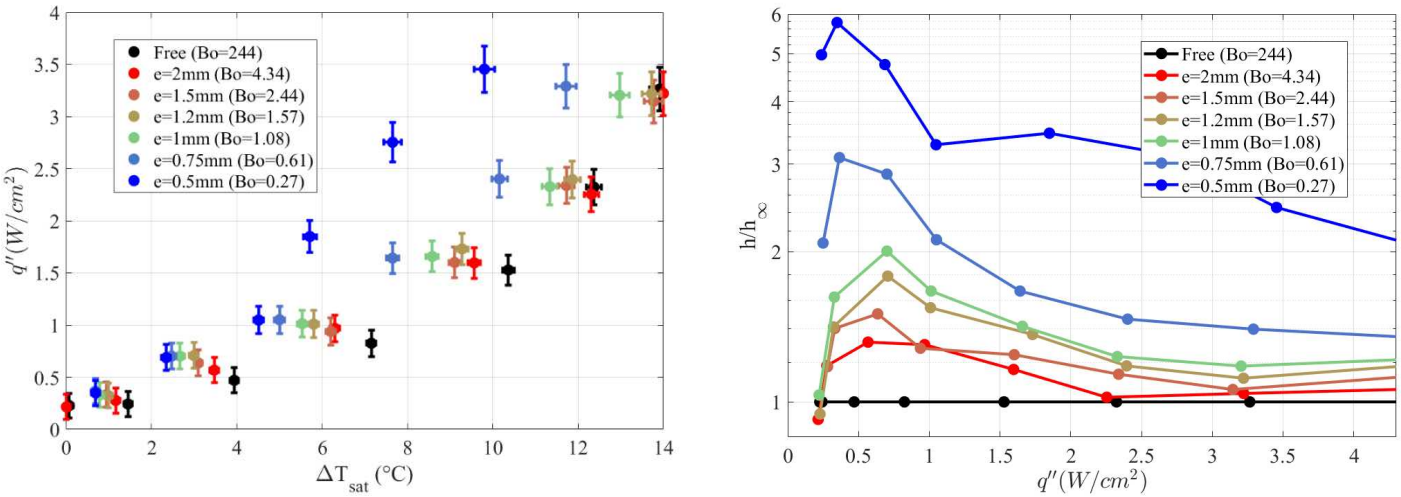

(A) *(B)*

Figure 11
(A) - Boiling curves at different confinements at low heat flux
(B) – Heat transfer coefficient comparison at low heat flux

hypothesis that in the free configuration case (where e=15mm) the fluid can be considered unconfined.

The difference in superheats between canal widths is not linear. Indeed, there is a larger gap between the confinements e=0.5mm and e=0.75mm than from all the other canal widths. Also, at lower heat flux the spread in wall superheat between all confinements is closer than for higher heat flux, from less than 2°C to more than 4°C. This decrease in wall superheat at a smaller canal width can be associated to the higher surface at the interface between the liquid-vapor phases, through bubble flattening and bubble coalescence inside the canal. Convection should also improve through confinement.

A ratio of the heat transfer coefficient at a given canal width compared to the one for the free configuration can be observed in **Fig. 11.B.** The data shown here is calculated with a thermocouple immersed directly in the fluid, in front of the thermocouples inside the heated plate. For the highest confined case e=0.5mm, the heat exchange is improved up to 600% at low heat flux. Once again, the impact of confinement on heat transfer coefficients is not linear.

Bonjour [4] found the same trends during his research on confined boiling, using R-113 fluid: small canal widths allow lower wall superheats than the free case. He also observed a peculiar result about the width of the canal: at the most confined cases (Bo=[0.08;0.33]) the

heat transfer coefficients go through a maximum value at *Bo*=0.19, then decrease again for *Bo*=0.08. This trend is not observed in the current research, but it is possible that the range of the confinement was simply not small-scale enough, as current experimental data is for *Bo*=0.27 at the lowest.

Ait-Ameur [13] witnessed the same phenomenon with R-113 fluid. The heat transfer coefficient increases at low heat flux with the reduction of canal width up until they reach an optimum for *Bo*=0.25 (where heat transfer increases up to 600%), then they decrease again as the canal width is further reduced.

As a partial conclusion for this range of heat flux, confinement provides a decrease in global wall superheats. The more the confinement, the lower the wall superheat.

2.4 – Fully developed nucleate boiling and coalescence on vertical plate

Data at the same vertical canal widths but at higher heat flux produce quite different results as shown in **Fig. 12**.

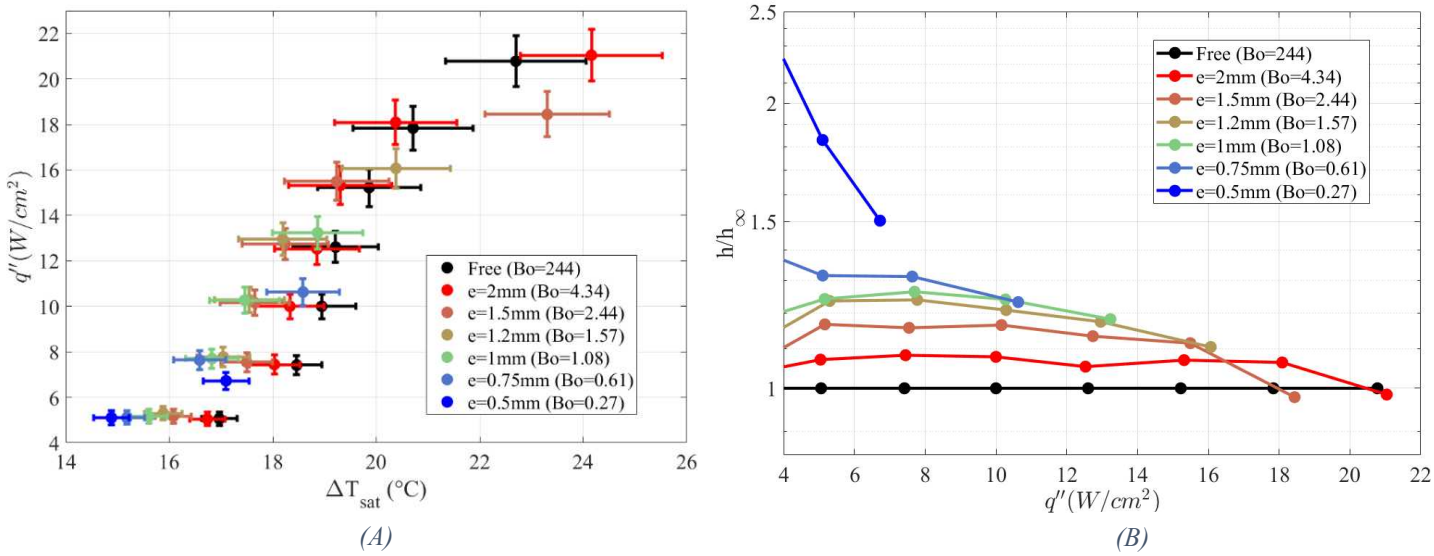

(A) *(B)*

Figure 12
(A) - Boiling curves at high heat flux
(B) – Heat transfer coefficients at high heat flux

This time, confinement does not lower considerably the wall superheat as seen in **Fig. 12.A**. On the contrary, at an increasing heat flux for an increasing canal width the boiling curve

presents a change in the slope. This trend is also clear through the heat transfer coefficients shown in **Fig. 12.B**, as they are clearly seen decreasing at higher heat flux.

It is noteworthy that only three series of points could achieve the maximum applied heat flux of 20 W/cm² at steady-state and without reaching critical heat flux. They correspond to the less confined cases such as the free configuration, *e*=2 mm and *e*=1.5 mm. For the other canal widths film boiling was reached at a lower heat flux. Because film boiling increases drastically the wall superheats in short periods of time, it prevented to measure higher heat flux at small canal widths for safety reasons.

Given that at higher heat flux there is more heat to evacuate from the plate, the confined cases restrict the access to the descending cold liquid compared to the free configuration. Hence the liquid-vapor mix in front of the plate heats up even more while ascending in the canal, making it harder for the cold liquid to reach the heated plate.

At 18 W/cm², it is interesting to notice that *e*=1.5 mm presents a noticeable increase in superheat (+3 °C) compared to *e* = 2 mm and the free configuration, while similar wall superheats between 5 and 16 W/cm². Moreover, as said before, this change in the slope is followed with the reaching of critical heat flux. This increase means that the confinement effect can be noteworthy at a canal width of 1.5 mm, but only at a high enough heat flux. If the same logic observed for other confinements is applied here, this means that the heat flux range of the study was not enough to display the limitations of confinement at *e*=2 mm. But for this study, it is possible to consider the *e*=2 mm case as a free configuration at this range of heat flux.

In the literature it is usually recognized that confinement limits heat exchange at high heat flux, this is not verified in the present research. But the existence of an inflexion point – which is shifted at a higher wall superheat for greater canal widths - is detected in this study. The authors believe that confinement does not limit heat exchange even at higher relative heat flux. More realistically, the critical heat flux appears for lower values in the confined cases, anticipating the shift to another boiling regime.

Finally, at the highest heat flux the critical heat flux could also be observed for canal widths smaller than *e*=1.5 mm, this was not the case for the free configuration case in **Fig. 9**. These points are not shown here and will be treated in a later section. Also, the boiling regimes reported in **Fig. 9** were also observed at the other canal widths, but the transitions between

regimes vary with confinement, this will be discussed in a later section through a regime map.

2.5 – Critical heat flux (CHF) on vertical plate

Focus is now shifted to the critical heat flux needed to reach film boiling. These data were obtained at increasing heat flux, unlike the previous study. The detection of film boiling was done through the thermocouple measurements coupled with visual observation. The thermocouples are responsive enough to measure significant temperature increases when film boiling is reached. Indeed, the procedure consisted in gradually increasing the heat flux until the wall superheat increased considerably faster during the data acquisition. Film boiling often coincides with the impossibility of reaching steady-state regime, with temperatures rapidly exceeding the maximum operational temperature of the testbench.

Results are shown in **Fig. 13**. Film boiling was achievable only for the most confined cases, for canal widths smaller or equal than e = 1.5 mm. The heat flux is measured at the center of the heated plate, as it was the location where the temperatures rose the fastest and heat flux increased the most during confinement.

There is a clear decreasing trend of critical heat flux with confinement. This is in line with the research found in the literature: several authors [4, 13, 34] observed the same behavior.

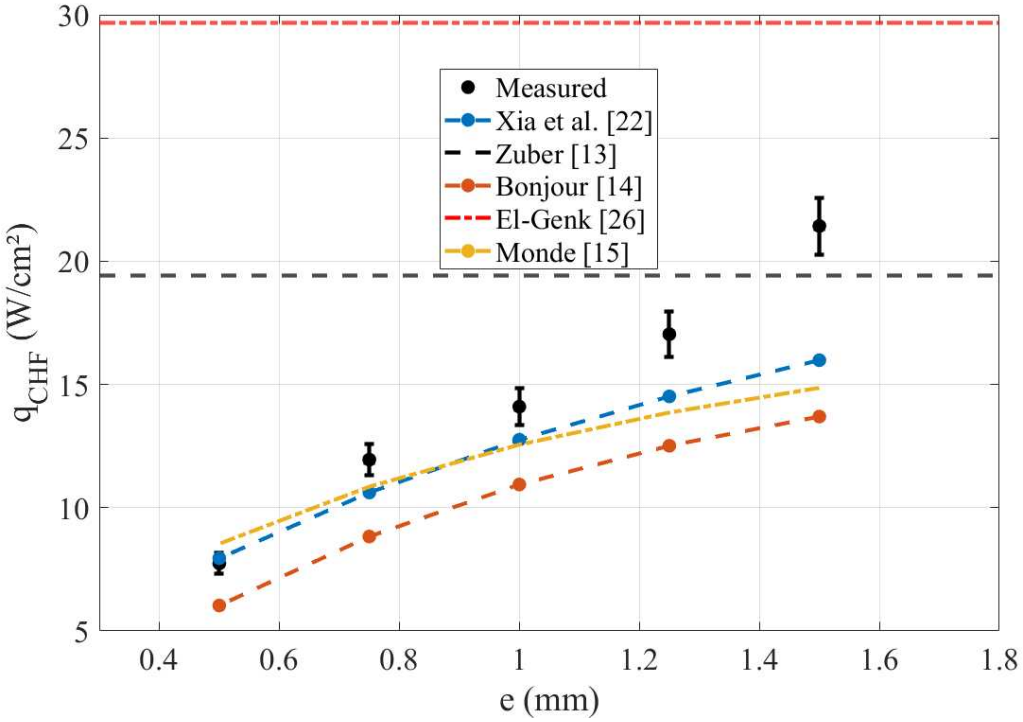

Figure 13 - Film boiling depending on confinement

Correlations from the literature have been added to compare current measurements to other studies, considering the pressure variations for each point. The Zuber [18] **(Eq. 13)** correlation does not include the confinement as a parameter, but it is the most widely used in boiling literature as a starting point for critical heat flux determination for an infinite upward horizontal plate. It is represented as a fixed value not depending on e at $q_{CHF}=19 W/cm^2$. Another value not depending on confinement is the one from El-Genk [31] **(Eq. 15)**, it is still included here as their study was also done with Novec 7000 but on a copper surface and at 0.85 bar. Seeing the trend of present data, it is reasonable to assume that their predicted value of $q_{CHF}=29 W/cm^2$ could very well be reached at higher canal widths or in the free configuration.

Xia et al. [34] developed a correlation with similar terms of the Zuber one, which has the aspect ratio *H/e* as a parameter for a vertical plate. Their correlation fits quite well with the current experimental data for smaller confinements, with an increasing relative error at higher canal widths up to 37%. The same is true for the Monde et al. [16] correlation, while the Bonjour and Lallemand [15] one presents a larger relative error at higher canal widths. These correlations do show marginally lower values of CHF, and this can be explained by boundary condition of the heated vertical plate in the testbench. In fact, on the sides of the heated plate

there is the Deltherm thermal insulation material (refer to **Fig. 2**, described in section **1.1**). On the sides of the heated plate - in front of the insulation material - cold fluid descends smoothly, as there is not an ascending hot flow there. This increases cold fluid supply from the sides, thus increasing heat transfer coefficients and retarding CHF.

On a physical level - for higher confinements such as e = 0.75 mm and especially e = 0.5 mm - even the shape of the bubbles is clearly flattened in the small canal width, increasing chances of coalescence as shown in **Fig. 14**. Vapor accumulation is thus greatly enhanced because of the smaller canal width, anticipating film boiling for a lower heat flux. This phenomenon is amplified in our system as both the bottom and sides of the canal are closed, meaning the only entry for cold liquid is the top of the canal – where vapor is ascending.

Finally, another set of experimental data can be compared to validate the values of critical heat flux for different confinements. The data taken at increasing heat flux in sections **2.3** and **2.4** could also reach critical heat flux at the highest heat flux for canal widths smaller or equal to e=1.5mm. This could be observed as a sharp decrease in heat transfer coefficient at a high enough heat flux. The results are shown in **Fig. 15**. The heat flux associated with the acute decrease in heat transfer coefficient correspond to the critical heat flux measured and shown in **Fig. 15**.

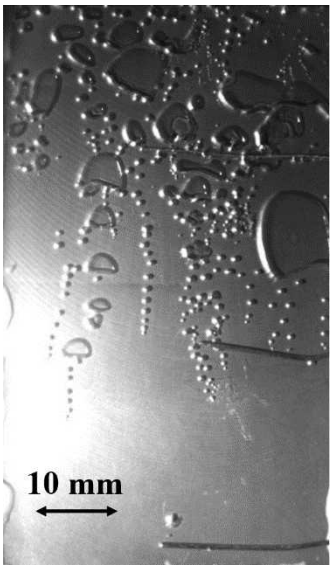

Figure 14 - Flattened bubbles at e=0.5mm

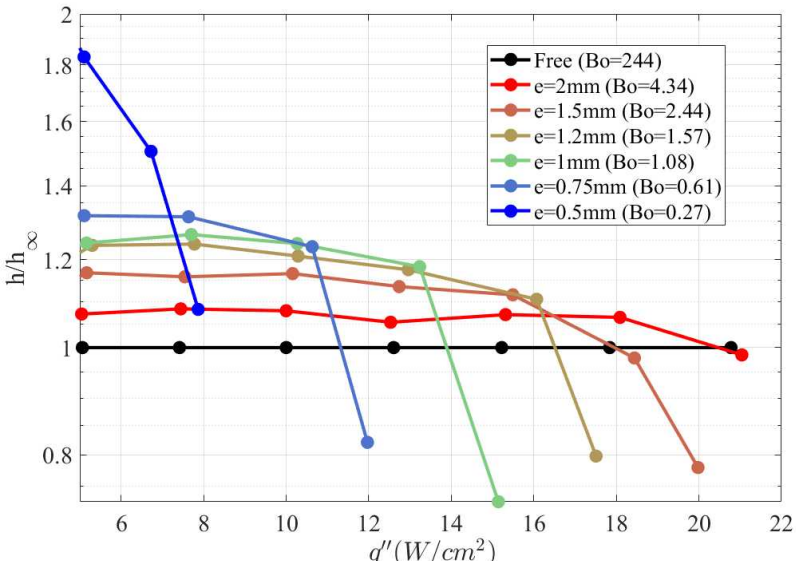

Figure 15 – Heat transfer coefficient near critical heat flux

2.6 - Influence of confinement on vertical plate boiling regimes

A stream map of the boiling regimes for the vertical plate has been experimentally obtained, the results are shown in **Fig. 16**. Plus, **Fig. 17** shows typical photos of the 3 boiling regimes.

The isolated bubbles regime starts at the 'Onset' heat flux data series on the graph, which represents the minimum heat flux needed for the activation of the first nucleation site. For a lower heat flux there is only natural convection. The 'Developed' data series corresponds to the point where nucleation site density becomes significant enough to cover the whole vertical surface. The 'Coalescence' series represents the minimum heat flux at which bubbles start to coalesce. Both these regimes are mainly recognized through optical visualization. Finally, critical heat flux data corresponds to that of section **2.5**.

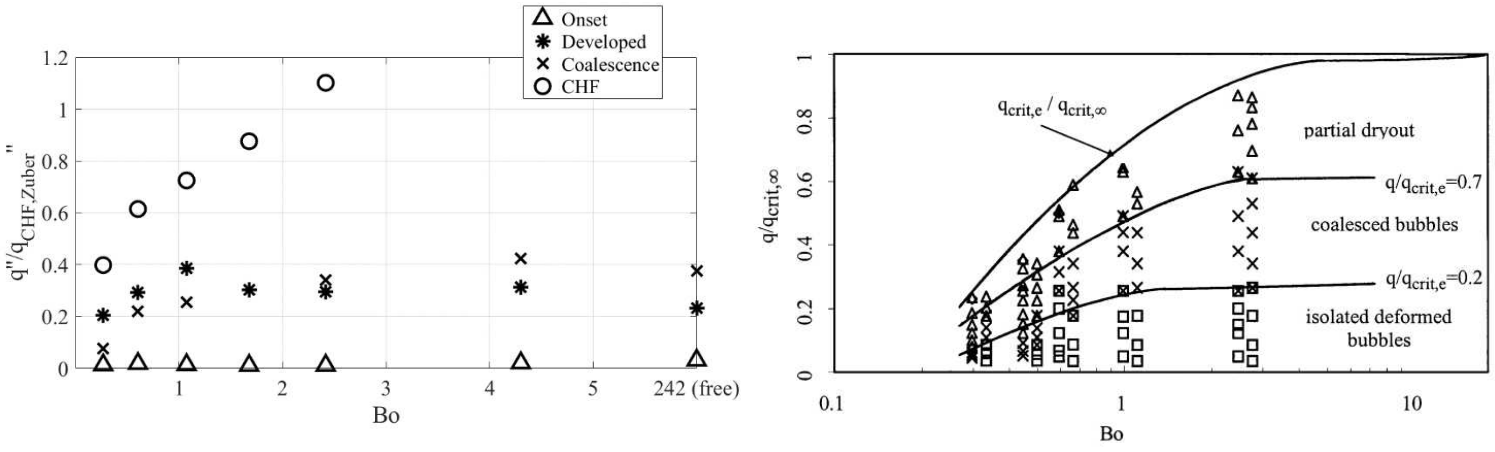

Figure 16 - Steam map of boiling regimes
A – Present study, B – Bonjour [56]

It is curious to observe that there is a crossing point between the coalescence and the nucleation points. For large canal widths, the heat flux needed to reach nucleation on the whole surface is always smaller than the one needed to reach coalescence. Inversely, for smaller canal widths coalescence is obtained with a smaller heat flux than for nucleation on the whole surface. This is because at small gap sizes (e<1mm) there is much less space for both the vapor and liquid phase to coexist and flow. Hence the vapor is entrapped between the heated surface and the wall. This flattens the vapor bubble and increases the probability of activating the neighboring sites then coalesce with them. This can happen before all the surface is covered in nucleation sites and the effect is even more important at very small gap sizes, where the isolated bubbles regime lasts only for very low heat flux. This can be

observed to the example of snapshots for confined boiling in **Fig. 17.B**, as coalescence is obtained on the higher part of the plate, before nucleation is present on the whole surface.

Somewhere between the heat flux associated to high coalescence and the critical heat flux, a partial dry out regime exists. But due to its erratic nature, it was too difficult to fix a requirement to use as a clear mean of identification of the start of the regime during testing.

Indeed, there was not a big visual difference between a partial dryout regime and the critical heat flux, which is why the thermocouples were used to recognize the latter. An example of critical heat flux in a confined case is shown in **Fig. 17.C**.

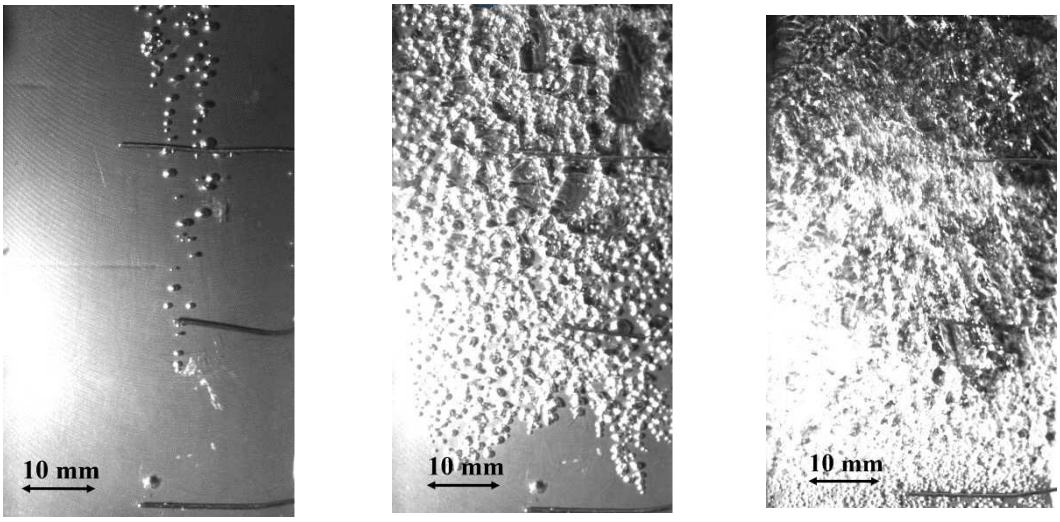

Figure 17 - Boiling regimes for confined boiling (e=0.5mm): isolated bubbles (A), coalescence (B) and film boiling (C)

These results show a very similar demeanor with the stream map shared by Bonjour et Lallemand with R113 fluid with a vertical plate [56]. This validates the overall trends observed in the study.

2.7 – Influence of the heating of one plate on the other

This original configuration representing the corner of a parallelepipedal heating element, with the two adjacent heated plates at a 90° angle, was also realized to highlight the influence of one plate on the other. To achieve this, it is useful to compare the boiling curves of the horizontal and vertical plates when the plates are heated on their own or simultaneously. Both plates simultaneous boiling represents a situation where a parallelepipedal heating element (such as components found in an electric vehicle) is cooled on more than one side. Moreover,

a juxtaposition of data for both the free case '∞' and for the smaller vertical canal width 'e=0.5mm' is given to check if it has an impact for both cases, even on the horizontal plate.

In **Fig. 18** are plotted the boiling curves of the horizontal plate, for when both plates are heated ('H+V' configuration) and when just the horizontal is heated ('H'). The free configuration is represented with the red cross markers, while when the vertical canal is confined in the blue points markers.

Up to 12 W/cm², there is little to no variation between all the data points (<1°C). For higher heat flux, corresponding to the fully developed boiling regime, some differences occur. First, when the horizontal plate is heated on its own, a change in the vertical canal width does not influence the heat exchange on the horizontal plate. On the other hand, the canal width does impact heat exchange when both plates are heated: when the vertical plate is confined, it

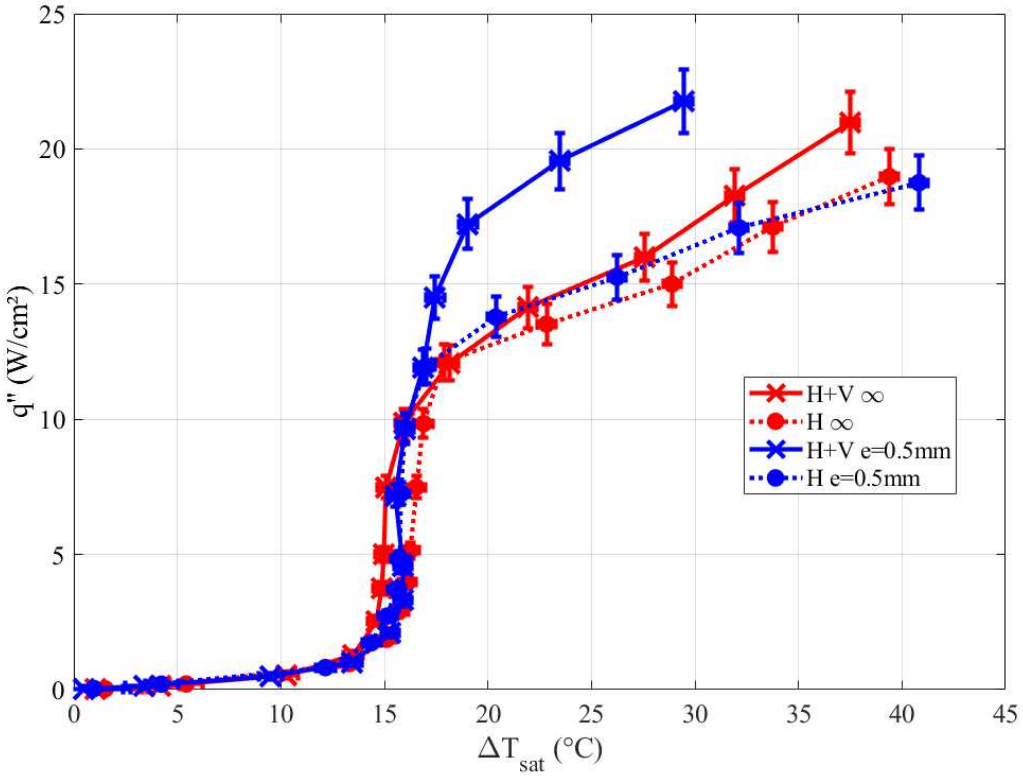

Figure 18 - Boiling curves for the horizontal plate in different configurations

lowers the wall superheat on the horizontal plate. The temperature difference between 'H+V ∞' and 'H+V *e*=0.5mm' reaches a maximum of 8°C at the highest heat flux, suggesting the impact of the vertical plate on the horizontal grows with heat flux. Indeed, the vertical plate influence is basically nonexistent for q''<12 W/cm².

Another takeaway from **Fig. 18** is that when both plates are heated, the horizontal one presents lower wall superheats than when it is heated on its own, independently of the

configuration. This is an interesting result, as it could be thought that because when both plates are heated there is a higher quantity of heat introduced in the system: this could increase wall superheats overall. Although direct visualization for the horizontal plate is not possible, it is fair to assume that the boiling flow created in front of the vertical plate induces some complex recirculation flows inside the system favoring the horizontal plate. This effect is more significant for the smaller vertical canal width. It means that in the free configuration - where there is enough space in front of the vertical heated plate - the vapor created in the canal has enough space to expand and condensate far enough from the horizontal plate, impacting less its heat transfer coefficient.

Focusing now on the difference of heat exchange for the vertical heated plate, **Fig. 19** shows the difference between when both plates are heated simultaneously and when the vertical plate is heated on its own. The data is given at two different vertical canal widths too.

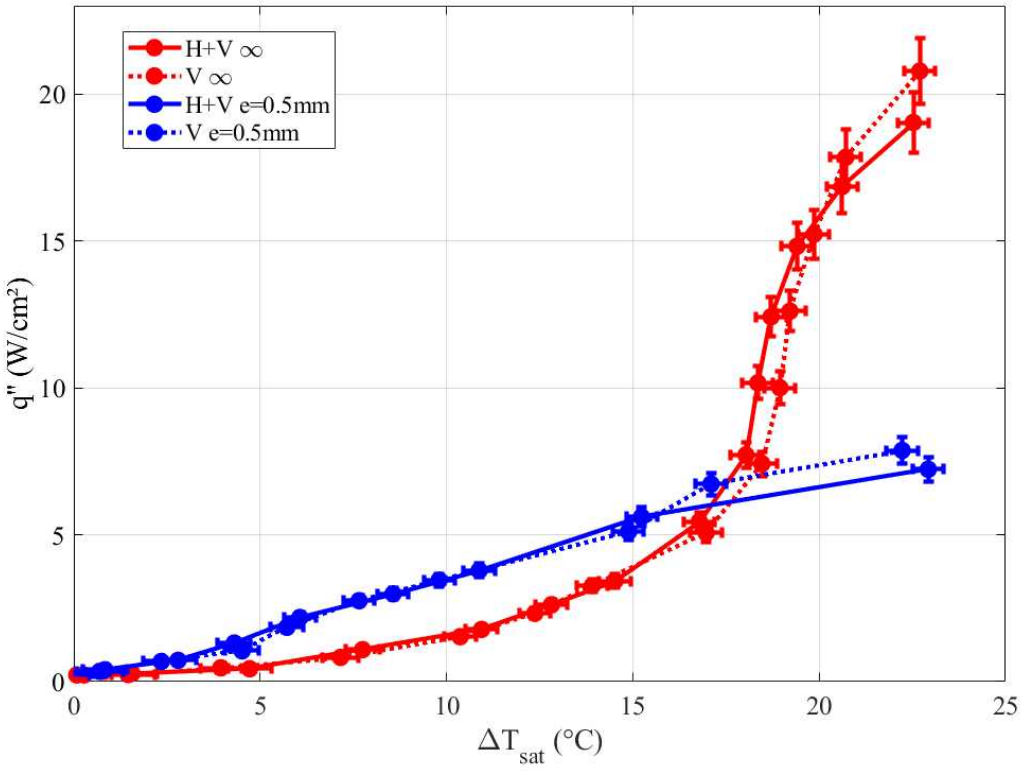

Figure 19 - Boiling curves for the vertical plate for different configurations

This time, the horizontal plate has no impact on the vertical plate's heat exchange. Indeed, both for the confined case and for the free configuration, the difference in the boiling curve remains inconsequential. It is also interesting to validate once again the effect of confinement, both when the vertical plate is heated on its own or with the horizontal plate. It lowers the wall superheats for heat flux up to 6 W/cm² compared to the free configurations,

but then it immediately reaches the partial dry-out regime, increasing the temperatures much faster.

Hence, although the horizontal plate has no significant effect on the vertical plate, the vertical plate does have a beneficial impact on boiling on the horizontal plate. For this reason, at the same overall heat flux density, it is recommendable to use both the horizontal and the vertical surfaces of the coin of a parallelepipedal heating element in immersion two phase cooling. A confrontation with the literature of these conclusions was not possible, as they are completely original.

Conclusion

A novel experimental testbench has been developed to study boiling of a dielectric fluid (Novec 7000) on both a horizontal and a vertical plate creating a 90° angle between them. The present study focuses on the validation of experimental results on this new experimental device on both plates, with an emphasis on the influence of confinement on boiling on the vertical surface. Confinement has been found to improve considerably heat exchange at low to medium heat fluxes (0-5 W/cm²), while at higher heat flux a limited to no improvement could be measured. Moreover, confinement lowers the critical heat flux. The temperature measurements were coupled with a visual study to identify boiling regimes depending on confinement. This allowed for the detection of a crossing point between coalesced bubbles and nucleation on the whole surface depending on heat flux, compared to the free configuration case. To conclude, simultaneous and isolated heating has been applied to both heated plates to examine the reciprocal influence of boiling on each: vertical plate improves heat exchange on the horizontal one, whereas horizontal plate has no effect on the vertical. Thus, for the same overall surface heat flux density it is beneficial to let boiling occur on both faces of a corner of a parallelepipedal heating element instead of favoring only one side for cooling.

Declaration of competing interests

None.

Acknowledgements

The authors would like to gratefully acknowledge the technical staff of the Laboratoire de Thermique et Energie de Nantes for their support in the conception, the manufacturing, installation and the tuning of the experimental setup: Gwenael Biotteau, Nicolas Lefèvre and Julien Aubril.

Annex

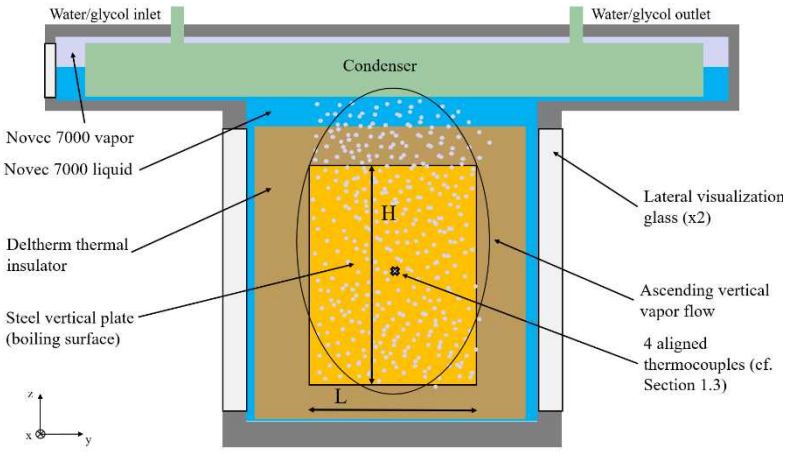

Figure A.1 – Frontal schematic view of the vertical plate

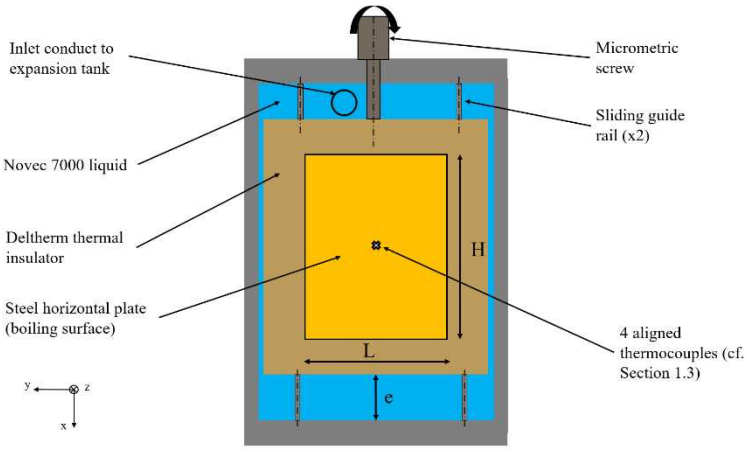

Figure A.2 - Upper schematic view of the horizontal plate

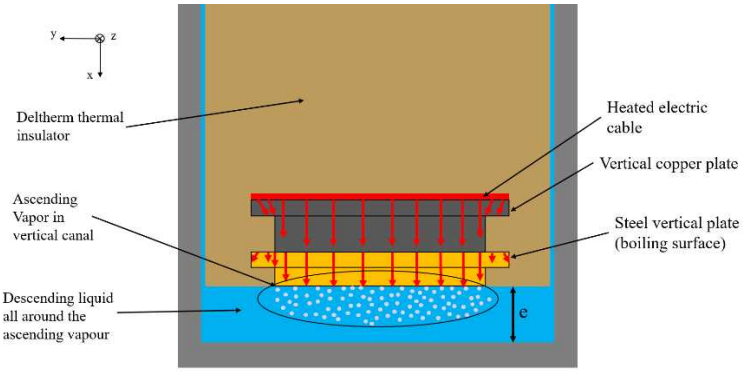

Figure A.3 – Section schematic view of the vertical plate in the free configuration

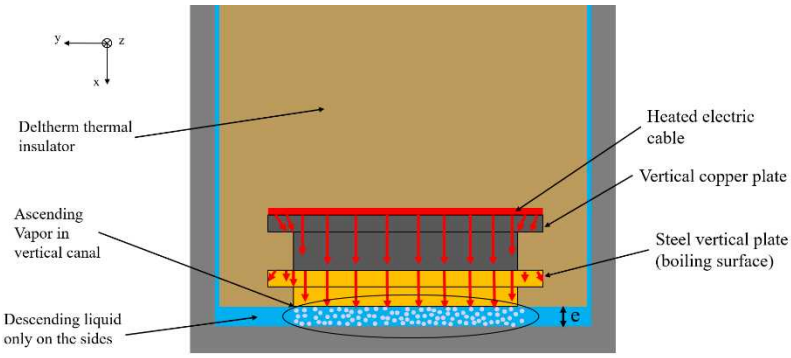

Figure A.4 - Section schematic view of the vertical plate in the confined configuration

References

[1] B. Gvozdic, On-Yu Dung, E. Alméras, P.M. van Gils, D. Lohse, S. G. Huisman, C. Sun, Experimental investigation of heat transport in inhomogeneous bubbly flow, Chemical Engineering Science 198 (2019) 260–267

[2] U. Sajjad, A. Sadeghianjahromi, H. M. Ali, C-C. Wang, Enhanced pool boiling of dielectric and highly wetting liquids – A review on surface engineering, Applied Thermal Engineering 195 (2021) 117074

[3] P. Chen, S. Harmand, S. Ouenzerfi, Immersion cooling effect of dielectric liquid and self-rewetting fluid on smooth and porous surface, Applied Thermal Engineering 180 (2020) 115862

[4] J. Bonjour, Amélioration des transferts de chaleur en ébullition naturelle convective par effet de confinement, PhD Thesis, Institut National des Sciences Appliquées de Lyon, 1996

[5] S. Wu, H. Dai, H. Wang, C. Sheng, X. Liu, Role of condensation on boiling heat transfer in a confined chamber, Applied Thermal Engineering 185 (2021) 116309

[6] S. Nukiyama, The maximum and minimum values of the heat Q transmitted from metal to boiling water under atmospheric pressure, International Journal of Heat and Mass Transfer 9 (1966) 1419-1433

[7] C-Y. Han, P. Griffith, The mechanism of heat transfer in nucleate pool boiling - Part I, International Journal of Heat and Masse Transfer 8 (1965) 887-904

[8] Y. Y. Hsu, On the size range of active nucleation cavities on a heating surface, Journal of Heat Transfer 84 (1962) 207-213

[9] K.C. Leong, J.Y. Ho, K.K. Wong, A critical review of pool and flow boiling heat transfer of dielectric fluids on enhanced surfaces, Applied Thermal Engineering 112 (2017) 999-1019

[10] S.C. Yao, Y. Chang, Pool boiling heat transfer in a confined space, International Journal of Heat and Mass Transfer 26 (1983) 841-848

[11] C. Xia, Z. Guo, W. Wu, Mechanism of boiling heat transfer in narrow channels, ASME Conference of Two Phase Flow and Heat Transfer 197 (1992) 111-119

[12] P. F. Rampisela, Étude expérimentale de l'ébullition en espace confiné, Grenoble INPG, 1993

[13] M. Ait-Ameur, Etude expérimentale de l'ébullition naturelle confinée : analyse des instabilités et des transferts thermiques, PhD Thesis, Institut National des Sciences Appliquées de Lyon, 2006

[14] N. Zuber, On the stability of boiling heat transfer, Transactions of the ASME 80 (1958) 711–720

[15] J. Bonjour, M. Lallemand, Effects of confinement and pressure on critical heat flux during natural convective boiling in vertical channels, International Communications of Heat and Mass Transfer 24 (1997) 191-200

[16] M. Monde, H. Kusuda, H. Uehara, Critical Heat Flux During Natural Convective Boiling in Vertical Rectangular Channels Submerged in Saturated Liquid, Transactions of the ASME 104 (1982) 300-303

[17] K.J.L. Geisler, A. Bar-Cohen, Confinement effects on nucleate boiling and critical heat flux in buoyancy-driven microchannels, International Journal of Heat and Mass Transfer 52 (2009) 2427–2436

[18] N. Zuber, The Hydrodynamic Crisis in Pool Boiling of Saturated and Subcooled Liquids, International Developments in Heat transfer (1961)

[19] M. S. El-Genk, M. Pourghasemi, Subcooled boiling critical heat flux of HFE-70 0 0 dielectric liquid on inclined rough Cu, International Journal of Heat and Mass Transfer 175 (2021) 121354

[20] S.C.P. Cheung, S. Vahaji, G.H. Yeoh, J.Y. Tu, Modeling subcooled flow boiling in vertical channels at low pressures – Part 1: Assessment of empirical correlations, International Journal of Heat and Mass Transfer 75 (2014) 736–753

[21] A. A. Alsaati, D. M. Warsinger, J. A. Weibel, A. M. Marconnet, A mechanistic model to predict saturated pool boiling Critical Heat Flux (CHF) in a confined gap, International Journal of Multiphase Flow 167 (2023) 104542

[22] Incropera, Dewitt, Begman, Lavine, Fundamentals of heat and mass transfer, Sixth edition (2007)

[23] A. Suszko, M. S. El-Genk, Dielectric liquids natural convection on small rough Cu surfaces at different orientations, International Journal of Heat and Mass Transfer 81 (2015) 289–296

[24] M. S. El-Genk, M. Pourghasemi, Experimental investigation of saturation boiling of HFE-7000 dielectric liquid on rough copper surfaces, Thermal Science and Engineering Progress 15 (2020) 100428

[25] M. Bahrami, Natural convection, https://www.sfu.ca/~mbahrami/ENSC%20388/Notes/Natural%20Convection.pdf

[26] S. Churchill, H. Chu, Correlating equations for laminar and turbulent free convection from a vertical plate, International Journal of Heat and Mass Transfer 18 (1974) 1323-1329

[27] G. Gan, General expressions for the calculation of air flow and heat transfer rates in tall ventilation cavities, Building and Environment 46 (2011) 2069-2080

[28] W. M. Rohsenow, A method of correlating heat transfer data for surface boiling of liquids, Technical report of Massachusetts Institute of Technology, Heat Transfer Laboratory, 5

[29] K.Stephan, M.Abdelsalam, Heat-transfer correlations for natural convection boiling, International Journal of Heat and Mass Transfer 23 (1980) 73-87

[30] H. K. Forster, N. Zuber, Dynamics of vapor bubbles and boiling heat transfer, American Institute of Chemical Engineering Journal 1 (1955) 531-535

[31] M. S. El-Genk, M. Pourghasemi, Experiments and correlations of saturation boiling of HFE-7000 dielectric liquid on rough inclined copper surfaces, International Journal of Heat and Mass Transfer 164 (2021) 120540

[32] L. A. Bromley, Heat transfer in stable film boiling, Chemical Engineering Proceedings 46 (1950) 221-227

[33] Y.P. Chang, Wave theory of heat transfer in film boiling, ASME Journal of Heat Transfer 81 (1959) 112

[34] C. Xia, W. Hu, Z. Guo, Natural Convective Boiling in Vertical Rectangular Narrow Channels, Experimental Thermal and Fluid Science 12 (1996) 313-324

[35] G. Liang, I. Mudawar, Review of pool boiling enhancement by surface modification, International Journal of Heat and Mass Transfer 128 (2020) 892:933

[36] Z. Wu, Z. Cao, B. Sundén, Saturated pool boiling heat transfer of acetone and HFE-7200 on modified surfaces by electrophoretic and electrochemical deposition, Applied Energy 249 (2019) 286–299

[37] R. Bertossi, N. Caney, J. A. Gruss, O. Poncelet, Pool boiling enhancement using switchable polymers coating, Applied Thermal Engineering 77 (2015) 121-126

[38] S. Mori, Y. Utaka, Critical heat flux enhancement by surface modification in a saturated pool boiling: A review, International Journal of Heat and Mass Transfer 108 (2017) 2534–2557

[39] D. Gorenflo, V. Knabe, V. Bieling, Bubble density on surfaces with nucleate boiling - Its influence on heat transfer and burnout heat flux at elevated saturated pressures, Proceedings of 8th International Heat Transfer Conference, Washington DC, vol. 4

[40] S. Michaïe, Experimental study of the fundamental phenomena involved in pool boiling at low pressure, PhD Thesis, INSA Lyon, 2018

[41] J. Du, C. Zhao, H. Bo, A modified model for bubble growth rate and bubble departure diameter in nucleate pool boiling covering a wide range of pressures, Applied Thermal Engineering 145 (2018) 407–415

[42] R. Kamatchi, S. Venkatachalapathy, Parametric study of pool boiling heat transfer with nanofluids for the enhancement of critical heat flux: A review, International Journal of Thermal Sciences 87 (2015) 228-240

[43] M. S. El-Genk, M. Pourghasemi, Experimental investigation of saturation boiling of HFE-7000 dielectric liquid on rough copper surfaces, Thermal Science and Engineering Progress 15 (2020) 100428

[44] U. Sajjad, A. Sadeghianjahromi, H. M. Ali, C-C. Wang, Enhanced pool boiling of dielectric and highly wetting liquids - a review on enhancement mechanisms, International Communications in Heat and Mass Transfer 119 (2020) 104950

[45] U. Sajjad, A. Sadeghianjahromi, H. M. Ali, C-C. Wang, Enhanced pool boiling of dielectric and highly wetting liquids – A review on surface engineering, Applied Thermal Engineering 195 (2021) 117074

[46] M. Misale, G. Guglielmini, A. Priarone, HFE-7100 pool boiling heat transfer and critical heat flux in inclined narrow spaces, International journal of refrigeration 32 (2009) 235-245

[47] C. Wang, W. Chang, C. Dai, Y. Lin, K. Yang, Effect of inclination on the convective boiling performance of a microchannel heat sink using HFE-7100, Experimental Thermal and Fluid Science 36 (2012) 143-148

[48] J.Weisman, S.Y.Kang, Flow pattern transitions in vertical and upwardly inclined lines, International Journal of Multiphase Flow 7 (1981) 271-291

[49] R. Sugrue, J. Buongiorno, T. McKrell, An experimental study of bubble departure diameter in subcooled flow boiling including the effects of orientation angle, subcooling, mass flux, heat flux, and pressure, Nuclear Engineering and Design 279 (2014) 182–188

[50] 3M, 3M Novec 7000 Engineered Fluid Datasheet, https://multimedia.3m.com/mws/media/121372O/3m-novec-7000-engineered-fluid-tds.pdf

[51] M. H. Rausch, L. Kretschmer, S. Will, A. Leipertz, A. P. Frö, Density, Surface Tension, and Kinematic Viscosity of Hydrofluoroethers HFE-7000, HFE-7100, HFE-7200, HFE-7300, and HFE-7500, Journal of Chemical Engineering Data 60 (2015) 3759−3765

[52] R. F. Gaertner, Photographic study of nucleate pool boiling on a horizontal surface, Transactions of ASME, Journal of Heat Transfer 87 (1965) 17-29

[53] N. Zuber, Nucleate boiling. The region of isolated bubbles and the similarity with natural convection, International Journal of Heat and Mass Transfer 6 (1963) 53-78

[54] Thibault Layssac, Contribution à l'étude phénoménologique de l'ébullition convective en mini-canal, PhD Thesis, INSA Lyon, 2018

[55] Van P. Carey, Liquid Vapor Phase Change Phenomena, CRC Press - Taylor and Francis Group, 2020

[56] J. Bonjour, M. Lallemand, Flow patterns during boiling in a narrow space between two vertical surfaces, International Journal of Multiphase Flow 24 (1998) 947-960